J. Fluid Mech. (2010), *vol.* 643, *pp.* 395–424.
doi:10.1017/S0022112009992060

Dual resonance in vortex-induced vibrations at subcritical and supercritical Reynolds numbers

J. M. DAHL[1]†, F. S. HOVER[1], M. S. TRIANTAFYLLOU[1] AND O. H. OAKLEY[2]

[1]Department of Mechanical Engineering, Massachusetts Institute of Technology, 77 Massachusetts Avenue, Cambridge, MA 02139, USA

[2]Chevron Energy Technology Company, 6001 Bollinger Canyon Road, Rm. L-4228, San Ramon, CA 94583, USA

(Received 13 January 2009; revised 7 September 2009; accepted 7 September 2009; first published online 5 January 2010)

An experimental study is performed on the vortex induced vibrations of a rigid flexibly mounted circular cylinder placed in a crossflow. The cylinder is allowed to oscillate in combined crossflow and in-line motions, and the ratio of the nominal in-line and transverse natural frequencies is varied systematically. Experiments were conducted on a smooth cylinder at subcritical Reynolds numbers between 15 000 and 60 000 and on a roughened cylinder at supercritical Reynolds numbers between 320 000 and 710 000, with a surface roughness equal to 0.23 % of the cylinder diameter. Strong qualitative and quantitative similarities between the subcritical and supercritical experiments are found, especially when the in-line natural frequency is close to twice the value of the crossflow natural frequency. In both Reynolds number regimes, the test cylinder may exhibit a 'dual-resonant' response, resulting in resonant crossflow motion at a frequency f_v, near the Strouhal frequency, and resonant in-line motion at 2 f_v. This dual resonance is shown to occur over a relatively wide frequency region around the Strouhal frequency, accompanied by stable, highly repeatable figure-eight cylinder orbits, as well as large third-harmonic components of the lift force. Under dual-resonance conditions, both the subcritical and the supercritical response is shown to collapse into a narrow parametric region in which the effective natural-frequency ratio is near the value 2, regardless of the nominal natural-frequency ratio. Some differences are noted in the magnitudes of forces and the cylinder response between the two different Reynolds number regimes, but the dual-resonant response and the resulting force trends are preserved despite the large Reynolds number difference.

Key words: separated flows, vortex streets

1. Introduction

The phenomenon of vortex formation behind a bluff body in crossflow U is known to occur over a very wide range of the Reynolds number ($Re = UD/\nu$, where ν is the kinematic viscosity of the fluid and D is the cylinder diameter), starting at $Re \approx 50$ and reaching up to at least Reynolds numbers of 10^8 and higher (Blevins 1990); the details of vortex formation – including the non-dimensional frequency, or the Strouhal number St, and the forces – are known to be highly

† Present address: Singapore–MIT Alliance for Research and Technology Centre, S16-05-08 3 Science Drive 2, Singapore 117543. Email address for correspondence: jdahl@smart.mit.edu

dependent on the Reynolds number. At a certain critical value of the Reynolds number, $Re \approx 250\,000$ for a smooth cylinder, it has been shown that the drag coefficient of the cylinder drops dramatically because of a transition of the cylinder's boundary layer from laminar to turbulent flow (Roshko 1961; Achenback 1968; Schewe 1983). Consequently, significant changes in the Strouhal frequency are found, resulting in an alteration of the vortex shedding characteristics (Bearman 1969). Large differences in the hydrodynamic lift on the cylinder have also been observed throughout this transition region. At critical Reynolds numbers, coherent vortex formation may cease altogether (Zdravkovich 1997). At Reynolds numbers significantly higher than the critical number, vortex shedding again becomes well established in the wake of the cylinder, although the wake is significantly narrower because of the transition of the boundary layer to a turbulent state, which causes movement of the separation points further downstream along the cylinder surface (Zan 2008).

When the cylinder is flexible or elastically mounted, the interaction of vortex shedding with the structural characteristics of the body can lead to significant vortex-induced vibrations (VIVs) in both the in-line and the crossflow direction. Crossflow amplitudes can reach values typically up to two diameters, with smaller values in the in-line direction. Since the Reynolds number plays such an important role in vortex formation on a fixed cylinder in steady crossflow, we must also consider the effect of the Reynolds number on a flexibly mounted cylinder, where the structure can dynamically interact with the fluid. In addition to theoretical interest, there are several applications, particularly in the ocean, where flexible structures encounter flow conditions which range from the subcritical to the supercritical regime. Data in the supercritical regime, however, are very sparse because large testing facilities must be used at great expense.

Several recent studies have illustrated the dependence of Reynolds number on the VIV of a cylinder constrained to motions in the crossflow direction at subcritical Reynolds numbers. Carberry, Sheridan & Rockwell (2005) showed a Reynolds number effect on both fluid forces and wake state transitions. Through flow visualization on the wake of a cylinder undergoing controlled oscillations, Carberry *et al.* (2005) showed that over a small range of subcritical Reynolds numbers, the phasing of vortex shedding may be only slightly dependent on the Reynolds number; however, a stronger dependence exists between the magnitude of forces exerted on the body and the Reynolds number because even a small variation of the shedding point can affect the vortex patterns. In the case of a freely vibrating cylinder in the subcritical-Reynolds-number regime, Govardhan & Williamson (2006) found that as the Reynolds number increased over their analysed range, the oscillation amplitude and lift forces acting on the cylinder were also found to increase. Although the mass-damping parameter has been shown to strongly affect the peak response of the cylinder, a normalization is used to collapse the data over a wide range of experiments and wide range of subcritical Reynolds numbers to isolate the Reynolds number effect on cylinder excitation. Klamo, Leonard & Roshko (2005) showed that the maximum amplitude of a cylinder oscillating in the cross-stream could be represented purely as a function of the system damping and the Reynolds number and determined the maximum amplitude that the cylinder could achieve at given Reynolds numbers.

In experiments near the critical Reynolds number and for various roughness scales of the cylinder surface, Ding *et al.* (2004) reported a remarkable increase in the crossflow response, in excess of two diameters; the critical regime over which this increase is noted depends significantly on the value of the roughness. Raghavan & Bernitsas (2007) used roughness to enhance the amplitude of vibration of a flexibly

mounted cylinder for energy extraction purposes near the critical-Reynolds-number regime. Ding *et al.* (2004) further explored the vortex-induced response of a cylinder allowed to vibrate in the transverse direction for Reynolds numbers much higher than the critical value and for three different roughness values. They found that amplitudes up to about 0.90 diameters can be observed; the shape of the response as a function of reduced velocity depends significantly on the roughness level.

Studies by Sarpkaya (1995), Jauvtis & Williamson (2004) and Dahl *et al.* (2007) have shown that when the cylinder is also free to oscillate in-line with the flow, the hydrodynamic forces can be much different than those observed for a cylinder oscillating only in the crossflow direction. The resulting transverse amplitudes of the cylinder can also be significantly different than in experiments in which in-line oscillations are not allowed. With combined in-line and crossflow motions of the cylinder, significant third-harmonic components of lift were observed by Jauvtis & Williamson (2004) and Dahl *et al.* (2007).

For long, slender ocean structures such as risers and mooring lines, which have a countable sequence of natural frequencies, distributed vortex-induced forces may excite several natural frequencies, often at very high mode number. In this case, there can be many differences between their vibratory response and the response of short, flexibly mounted cylinders, including the formation of travelling waves, and multiple-frequency excitation, especially in sheared currents. Certain features of the response of long structures, however, are similar to those observed in laboratory experiments. Field experiments by Vandiver *et al.* (2006) and Vandiver, Jaiswal & Jhingran (2009) on a long, flexible pipe exhibited cylinder motions and third-harmonic force components similar to those observed by Dahl *et al.* (2007). Lucor, Mukundan & Triantafyllou (2006), Triantafyllou *et al.* (2007), Vandiver *et al.* (2009) and Mukundan, Hover & Triantafyllou (2009) showed that typical figure-eight shapes, seen in the two-degree-of-freedom response of a rigid cylinder, are also found in the travelling waves along a long, flexible pipe, accompanied by large third harmonics in the lift force.

The previously mentioned laboratory studies of combined in-line and crossflow VIV have been limited to subcritical Reynolds numbers. A study by Allen & Henning (1997) conducted at the David Taylor Model Basin was successful at showing that combined in-line and crossflow VIV are significant through the critical and supercritical regions of Reynolds numbers. In this experiment, flexible pipes were towed through the basin, and the oscillations of the pipes were observed. The reported study was fairly small in scope however, focusing primarily on the existence of vibrations at high Reynolds number and the effect on drag coefficients, rather than a systematic study of the vibratory response with respect to the reduced velocity. The study concluded that significant crossflow vibrations occur across the Reynolds number range tested and that in-line vibrations occur with smaller amplitudes.

The purpose of this paper is to study the effect of the Reynolds number on the VIV of cylinders in combined crossflow and in-line motion through a comparison of two experiments performed in towing tanks at subcritical and supercritical Reynolds numbers.

2. Experimental description

The basic apparatus consists of a flexibly mounted cylinder of diameter D placed within a crossflow with velocity U. The cylinder is mounted on springs in the crossflow direction, providing a nominal natural frequency in water, f_{ny}, and in the in-line direction, providing a nominal natural frequency in water, f_{nx}. We define

Crossflow amplitude ratio	$\frac{A_y}{D}$
In-line amplitude ratio	$\frac{A_x}{D}$
Nominal reduced velocity	$V_{rn} = \frac{U}{f_{ny} D}$
True reduced velocity	$V_r = \frac{U}{f_y D}$
Nominal natural-frequency ratio (in water)	$\frac{f_{nx}}{f_{ny}}$
Mass ratio	$m^* = \frac{m}{\rho \pi \frac{D^2}{4} S}$
Damping ratio	$\zeta = \frac{b}{4\pi(m + m_a) f_{ny}}$
Reynolds number	$Re = \frac{U D}{\nu}$

TABLE 1. Non-dimensional parameters for combined in-line and crossflow VIVs.

the relevant nominal non-dimensional parameters in table 1. Vortex shedding behind the cylinder will cause a vibratory response of the cylinder. In the case of repeatable response motions, the cylinder typically exhibits a nearly sinusoidal response in both the in-line and the crossflow direction. Remaining consistent with the definitions of Jauvtis & Williamson (2004), we define crossflow motion y and in-line motion x in (2.1) and (2.2), where θ is the phase difference between in-line and crossflow motions. The phase θ determines the particular orbit shape of cylinder motion in a reference frame fixed to the tow carriage. Once the cylinder response is established, we can define the relevant non-dimensional parameters governing the cylinder response as given in table 1:

$$y = A_y \sin(2\pi f_y t), \tag{2.1}$$

$$x = A_x \sin(2\pi f_x t + \theta). \tag{2.2}$$

In a system with both crossflow and in-line motions, it is possible to have different structural parameters for each direction of motion. In general, the system mass for a particular direction is denoted by m; the damping is denoted by b; and the spring constant is denoted by k. The subscripts y and x are used to signify the crossflow and in-line directions, respectively. In both experiments, the natural frequency of the system is determined by perturbing the still system with the test cylinder submerged in water. Since the experiment is done in water, the measured natural frequency and system damping are altered by an added mass, denoted as m_a. This added mass is estimated by the ideal added mass associated with a cylinder accelerating in a potential flow, since the natural frequency is measured with the cylinder submerged in water, similar to the practice of Jauvtis & Williamson (2004). The fluid is considered to have density ρ and kinematic viscosity ν.

Transitions in the state of the cylinder boundary layer and the cylinder wake are strongly dependent on the Reynolds number. To be consistent with previously published results, we follow the definitions for transitions found in Roshko (1961), all

based on the observed changes in the drag coefficient of a steadily towed cylinder as a function of the Reynolds number. For a smooth cylinder in a crossflow, the large change in drag coefficient that occurs near the critical Reynolds number, $Re \approx 250\,000$, is defined as the 'initial transition'. For Reynolds numbers below the initial transition, the regime is labelled as 'subcritical'. Similarly, for Reynolds numbers larger than the initial transition, the regime is called 'supercritical'. For smooth cylinders and Reynolds numbers much higher than the critical Reynolds number, typically above $Re \approx 3\,500\,000$, the drag coefficient recovers a nearly steady value of around 0.6 or 0.7; this region defines the 'transcritical regime'.

In the present high-Reynolds-number experiments, a slightly roughened cylinder was used instead of a smooth cylinder. For rough cylinders there are three important changes to the drag coefficient transition. As the roughness increases (*a*) the critical Reynolds number decreases monotonically; (*b*) the drop in drag coefficient at the critical Reynolds number also decreases monotonically; and (*c*) the transcritical range begins at decreasing values of Reynolds number with the steady value of the drag coefficient increasing monotonically. Hence, for a rough cylinder the subcritical and the supercritical (and also the critical and the transcritical) regimes are defined with respect to corresponding changes in the curve of the drag coefficient of a steadily towed cylinder as a function of the Reynolds number.

2.1. *Subcritical-Reynolds-number experiments*

Low-Reynolds-number experiments were conducted in the MIT Towing Tank testing facility. The testing tank is 2.4 m wide and 1.2 m deep and has a useful test length of 22.5 m. The experiments are also described in Dahl, Hover & Triantafyllou (2006), and a detailed description of the test apparatus is given therein. The apparatus consisted of a large framework supporting a linear bearing system that allowed a test cylinder to vibrate in combined in-line and crossflow oscillations. Mechanical springs were used to tune the natural frequency of the structure in both directions, and six nominal natural-frequency ratios were tested over a range of reduced velocities, where the nominal natural-frequency ratio is defined as the measured in-line natural frequency over the measured crossflow natural frequency, both in water. Since there was damping in the apparatus because of the use of roller bearings, linear motors were used to help reduce damping in the vibrating system. The linear motors utilized velocity feedback from the test cylinder motions in order to output a force as a function of the velocity of the cylinder. The output motor force accounted for both linear damping and friction. The motor parameters were tuned to ensure positive damping in the system. A more detailed description of the error analysis for this method is given by Dahl *et al.* (2006).

The test cylinder used was a smooth cylinder, 76.2 mm in diameter. The apparatus was tuned to nominal natural-frequency ratios of 1, 1.22, 1.37, 1.52, 1.67 and 1.9 by adjusting mechanical springs in the in-line and crossflow directions. The cylinder was towed over a range of nominal reduced velocities between 3 and 12. The Reynolds number ranged from 15 000 to 60 000, depending on the particular test run. Dynamic lift and drag forces were measured using a piezo-electric force sensor, and amplitudes were measured with a linear potentiometer attached to the moving test cylinder. The mass ratio of the cylinder in the in-line and crossflow directions ranged between 3 and 6, depending on the particular frequency ratio. The exact values of mass ratio for each direction have been given by Dahl *et al.* (2006). Unlike the experiments of Jauvtis & Williamson (2004), where mass ratios were equal in both directions, the mass ratio was slightly smaller in the in-line direction than in the crossflow direction

for these experiments, since the in-line bearing system rode on the crossflow bearing system. The total system moving mass was slightly smaller in the in-line direction than in the crossflow direction. Additionally, in order to achieve the desired frequency ratios, the system needed to be tuned to different natural frequencies. The change in natural frequency was accomplished by changing the number of springs attached to the test apparatus. The mass of the springs contributed a significant portion of effective mass to the total system; hence changes in the natural frequency of the system resulted in slight changes to the mass ratio.

The study of Jauvtis & Williamson (2004) showed that the mass ratio can play a very important role in defining the response of the system, especially when the mass ratio is very close to one. Lower mass ratios and damping typically result in a cylinder response with larger amplitudes of motion and a widening of the response range over nominal reduced velocity. Because of the constraints of the experimental apparatus used in the low-*Re* experiments, it was not possible to keep the mass ratio constant while varying the nominal natural-frequency ratio, but efforts were made to keep the mass ratio and the damping as low as possible. Significant changes in the response curves can be attributed to changes in the nominal frequency ratio, based on comparisons with Sarpkaya (1995) and studies of the wake by Jeon & Gharib (2001).

2.2. *High-Reynolds-number experiments*

The high-Reynolds-number experiments were performed in the deep towing basin at the Institute for Ocean Technology at Memorial University in St. John's, Canada. The basin is 200 m long, 12 m wide and 7 m deep. Figure 1 shows a schematic drawing of the test apparatus used in the high-Reynolds-number experiments. The test apparatus consists of a large framework of I-beams that support the freely vibrating test cylinder as it is towed. The apparatus is designed to test conditions of forced cylinder motions in the crossflow direction and freely vibrating motions in the crossflow and in-line directions.

The freely vibrating apparatus consisted of (*a*) a system of linear bearings that allowed motion of the test cylinder framework in the vertical (crossflow) direction, (*b*) a spring-mounted towbar attached on pivots that allowed cylinder motion in the in-line direction and (*c*) a motor-controlled damping mechanism to adjust the equivalent structural damping of the apparatus. The linear rail and bearings are labelled in figure 1 on the downstream section of the test apparatus. Two vertical struts connected the moving test apparatus to the linear rails. The vertical struts also connected the system to springs that were used to tune the crossflow natural frequency of the structure. A chain and sprocket connected the damping control motor to the vertical struts. The test cylinder spanned the width between the vertical struts.

Two additional vertical struts were also located upstream from the cylinder, allowing a pivoted connection point for the two towbars. The forward vertical struts were mounted to actuators which could drive the struts with a controlled motion. When the test cylinder vibrates freely in the crossflow direction, the actuators are used with a feedback system to synchronize the motion of the forward struts with the motion of the downstream struts. The position of the aft struts was measured directly to provide the control input for the forward struts. This ensured that the towbars remain horizontally level during the oscillations, minimizing any rotation of the test cylinder. Previous experiments had shown that when the towbars were allowed to be inclined, the results were affected significantly. The towbars could be mounted in a rigid beam condition to restrict vibrations to the crossflow direction only, or springs could be added to the towbar in order to allow free in-line vibration. The springs on the towbars were adjusted to tune the nominal natural-frequency ratio of the system.

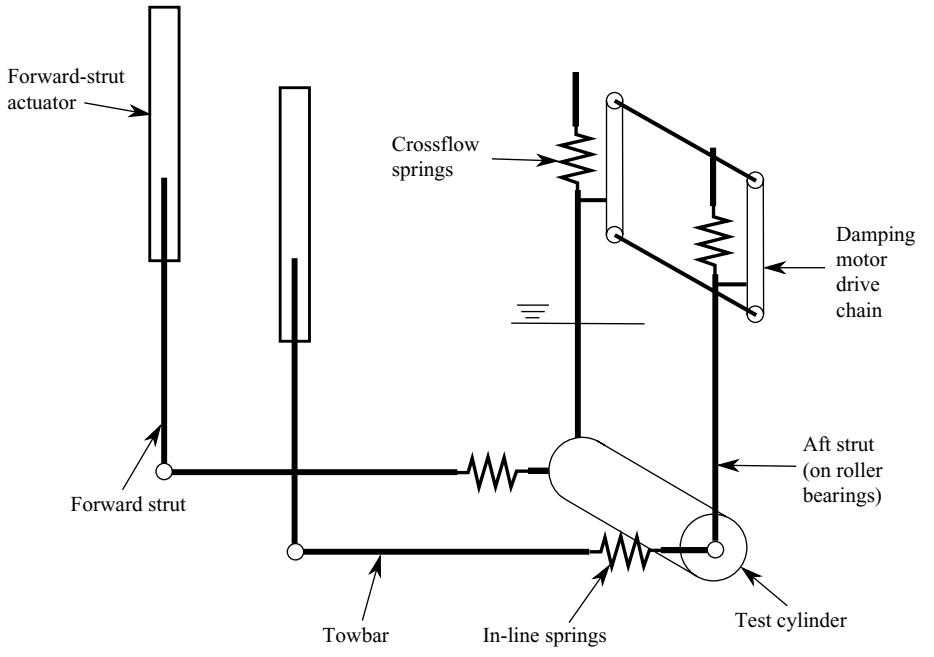

FIGURE 1. Schematic of high-Reynolds-number test apparatus. The apparatus connects to the Memorial University's towing basin carriage.

The presence of the towbar and forward struts in the experiments introduced a possible source of upstream disturbance to the incoming flow as seen by the cylinder. In order to characterize the effects of the towbar, the cylinder was towed in both a forward (towing) and a backward (pushing) configuration. If the forward-strut actuator was not activated, the system was inherently stable in the towing configuration and unstable in the pushing configuration, since the towbars were allowed to pivot at the connection to the forward strut. It was observed that the cylinder exhibited growing amplitude cylinder motions when moving in the pushed mode without the forward-strut actuator activated. In the towed mode, the cylinder exhibited no VIV motions without the forward strut activated. It is significant that when the forward-strut actuator control was activated, the towing configuration and the pushing configuration exhibited statistically identical cylinder responses. Since the response of the cylinder was the same in the pushed configuration and the towed configuration, any effect of the tow bars on the incoming flow was not found to affect the resulting cylinder response.

Damping exists in the test apparatus in the form of linear structural damping owing to flexure of the structural components, Coulomb friction in the linear bearings and additional hydrodynamic damping because of the submergence of the vertical struts and towbars. Similar to the low-Reynolds-number experiments, a motor is used with velocity feedback to reduce the structural damping in the system. Figure 1 shows the chain and sprocket connecting the damping motor to the vertical struts. Using feedback from the velocity of the test cylinder, the damping motor outputs a force in the direction of the velocity that is linearly proportional to the velocity. The feedback is tuned to ensure that the total system still retains a positive structural damping. No damping compensation was used in the in-line direction.

In order to characterize system damping, a series of pluck tests were done with and without the test cylinder attached. The force exerted by the damping motor on the

test apparatus frame was measured between the connection of the damping motor to the test frame. With the test cylinder attached, it was possible to measure both the hydrodynamic force F_H acting on the cylinder only and the damping compensation force F_D exerted by the damping motor. Assuming linear structural damping, the equation of motion appears as in (2.3), where m is the total moving mass of the system, b the linear damping of the system, k the system spring constant, y the time dependent position and F_R any residual forcing because of nonlinear damping (e.g. Coulomb friction forces, hydrodynamic forces on the submerged struts):

$$m\ddot{y} + b\dot{y} + F_R + ky = F_H + F_D. \tag{2.3}$$

An equivalent system damping b_{eq} can be defined by first finding the total damping force, consisting of the sum of the structural damping force $b\dot{y}$, the nonlinear damping force F_R and the compensation force $-F_D$; by equivalent linearization one can define an equivalent damping b_{eq} such that

$$b_{eq}\dot{y} \approx b\dot{y} + F_R - F_D, \tag{2.4}$$

where the expression $x(t) \approx y(t)$ means a least square approximation of $x(t)$ to $y(t)$. If we find the part of the hydrodynamic force in phase with velocity F_{H-v}, then, again in the least square sense, (2.3) and (2.4), provide

$$b_{eq}\dot{y} \approx F_{H-v}. \tag{2.5}$$

It is very important that the total equivalent damping b_{eq} is positive; otherwise the character of the self-excited VIV is altered. Since we measure directly the hydrodynamic force on the cylinder, we can calculate the force in phase with velocity and hence the total hydrodynamic damping, which was always found to be relatively small but positive, typically around 3 % of critical. This also guaranteed that the added energy with the motors did not result in spurious vibrations. As an additional precaution, the force provided by the motors was measured directly as well.

The following results were obtained. Without the test cylinder attached and for plucked tests, the linear damping constant for the system was determined to be equal to 980 kg s^{-1}. With the test cylinder attached and assuming an added mass coefficient of one for the plucked test cylinder in water, the residual forces were estimated to be (a) 24N of constant Coulomb friction opposing the velocity of the apparatus and (b) $278\dot{y}|\dot{y}|$N of hydrodynamic damping because of the presence of the struts and towbars in the water. The damping compensation system was only set to offset half of the linear damping constant, resulting in a compensated linear damping constant of 490 kg s^{-1}. As a percentage of critical damping, the equivalent damping coefficient caused by Coulomb friction is negligible, below 0.1 %, while the nonlinear damping coefficient is directly proportional to the amplitude of response, and its maximum value is less than 2 % of critical.

The test cylinder used was a 6.328 m long aluminum pipe with a 0.325 m diameter, resulting in an aspect ratio of 19.5. The pipe housed a five-component force dynamometer for measuring lift and drag forces on the cylinder. Cylinder motions were measured using accelerometers attached to the rigid test cylinder. The mass ratio of the freely vibrating system in the crossflow direction was 1.65, while the in-line mass ratio was 1.22. Similar to the low-Re experiments, the in-line moving mass was slightly smaller than the crossflow moving mass, since the towbars are included in the mass moving in the crossflow direction, while they are not included in the mass moving in the in-line direction. In the high-Re experiments, the mass of the springs did not contribute significantly to the effective moving mass of the

Ratio	f_{ny} (Hz)	ζ_y (%)	ζ_x (%)
0.77	1.53	1.9	5.8
1.55	1.53	1.9	2.9
1.63	1.33	2.2	3.2
2.23	0.97	3.0	3.2

TABLE 2. Frequency and damping properties for high-*Re* experiments. Reported damping ratios are based on linear damping only.

system; therefore the mass ratios were held constant across the range of nominal natural-frequency ratios.

The system was tuned to four nominal natural-frequency ratios of 0.77, 1.55, 1.63 and 2.23. The cylinder was towed at several speeds for each nominal frequency ratio over a small range of nominal reduced velocities. The Reynolds number ranged between 320 000 and 710 000, depending on the particular run. Table 2 shows the measured system properties, assuming a system with linear damping. To the linear damping values shown, we must add the Coulomb friction which is found to be negligible and the viscous damping which is less than 2 % of critical and directly proportional to the amplitude of response.

In the high-Reynolds-number experiments, a roughened cylinder was used rather than a smooth cylinder. In ocean applications, flexible cylinders become rough because of the corrosive effects of the environment, marine growth or both. In addition to this practical consideration, smooth cylinders operating close to the critical Reynolds number of around 250 000 can be considered 'pathological' in the sense that their responses are very sensitive to even small amounts of roughness or turbulence in the oncoming stream. Ding *et al.* (2004) found that smooth cylinders allowed to vibrate in the crossflow direction only undergo very large vibrations, with amplitude in excess of two diameters, very close to the critical Reynolds number (250 000); rough cylinders would also exhibit such large response over a short parametric range at earlier Reynolds numbers, corresponding to earlier transition in the boundary layer. On the contrary, just beyond the transition Reynolds number, perfectly smooth cylinders, in the sense of having roughness smaller than the thickness of the sublayer, exhibit no vortex-induced response; this was first reported in Allen & Henning (1997). Ding *et al.* (2004) found the same result for smooth cylinders allowed to vibrate in the crossflow direction, while roughness causes a re-emergence of large vibratory response. A smooth cylinder was first tested in the present experiments, and no vibratory response was initially found in the supercritical regime; however, even a small amount of surface roughness, or turbulence in the oncoming stream generated through upstream-placed screens, would cause the cylinder to vibrate.

It was decided to use a small roughness to avoid the noted sensitivity at the critical regime and emulate nearly transcritical flow conditions. Szechenyi (1975) showed that for a stationary cylinder in a crossflow, an equivalent supercritical flow may be obtained through an artificial increase in the Reynolds number by varying grades of roughness; however James, Paris & Malcolm (1980) found that the size of surface roughness with respect to the cylinder diameter has a large effect on the resulting drag coefficient. Additionally, Shih *et al.* (1993) found that a sufficiently rough surface can increase the spanwise coherence and fluctuating lift force amplitude; roughness will also increase the drag coefficient. Zan & Matsuda (2002) showed that fluid turbulence or roughness on the cylinder will result in higher drag coefficients, post-transition.

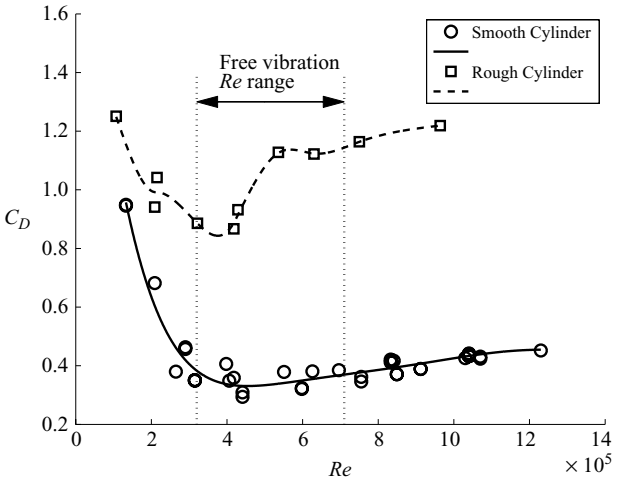

FIGURE 2. Drag coefficients for the smooth and roughened fixed cylinder in crossflow.

As a result, the choice was made to employ a roughness that is sufficiently small to keep the stationary cylinder drag coefficient less than $C_D \approx 1.2$ over the tested Reynolds numbers. To achieve the desired roughness, a fibreglass sleeve was fitted over the cylinder, covered in sand particles with a statistical average of the top one tenth of particle heights equal to 0.0023 of the cylinder diameter (0.23 % roughness). As shown in figure 2 the smooth cylinder drag coefficient shows a large drop at around $Re \approx 200\,000$, with a minimum value of the drag coefficient close to 0.30; the transcritical regime is well beyond the regime we tested. For the rough cylinder, the critical Reynolds number has moved to a value of around 120 000, and transcritical conditions start at around $Re \approx 450\,000$. The minimum value of the drag coefficient is around 0.85, while the steady value in the transcritical regime is around 1.1.

3. Comparison of subcritical and supercritical experiments

Because our supercritical tests are much sparser than the subcritical tests, we opted to present the results side by side. This helps identify trends, differences and similarities between the properties of the supercritical regime, which are largely unknown, and the better-established properties of the subcritical regime. As we show in this section, although there is significant difference in the Reynolds number, the principal features of the responses at the subcritical and the supercritical regime are found to be very similar.

In figure 3, the time traces for three pairs of the subcritical and supercritical cases are shown. Each high- and low-Re pair was selected to have nearly equivalent reduced velocities of 5.5, 5.9 and 6.5, respectively.

In each case there was a significant, narrowband motion response of the cylinder in the crossflow (y) direction and a narrowband response in the in-line (x) direction but with half the period relative to the crossflow direction. In all shown cases, the crossflow cylinder motion has nearly constant amplitude throughout the run. It is typical for the higher-Reynolds-number cases to display a lower crossflow amplitude than the lower-Reynolds-number cases. This trend is in agreement with results of cylinders allowed to vibrate only transversely (Ding *et al.* 2004), where the maximum

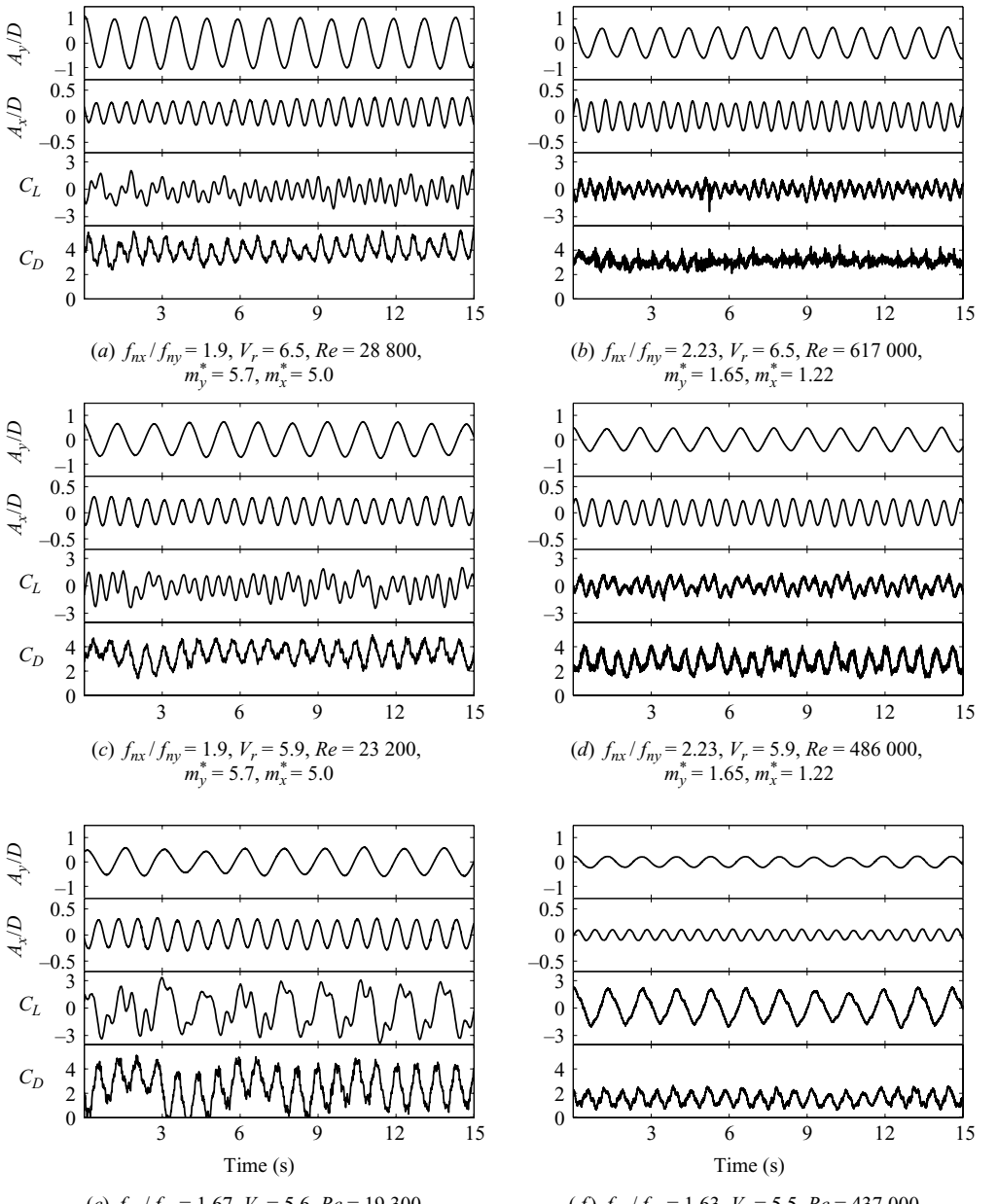

FIGURE 3. Time traces of motion and force signals for low- and high-Reynolds-number experiments at similar reduced velocities and nominal natural-frequency ratios. A significant third-harmonic force is noted in both lift signals for $V_r = 6.5$, while the third harmonic is significantly weaker at $V_r \approx 5.5$. Amplitudes are typically smaller for the higher Reynolds numbers.

amplitude at the supercritical Reynolds number was about 0.90 diameters, while at subcritical values the amplitude is often in excess of 1.2 diameters.

The frequency content of the lift force is better illustrated in figure 4, which provides for the lift signals shown in figure 3 the following quantities: (*a*) the

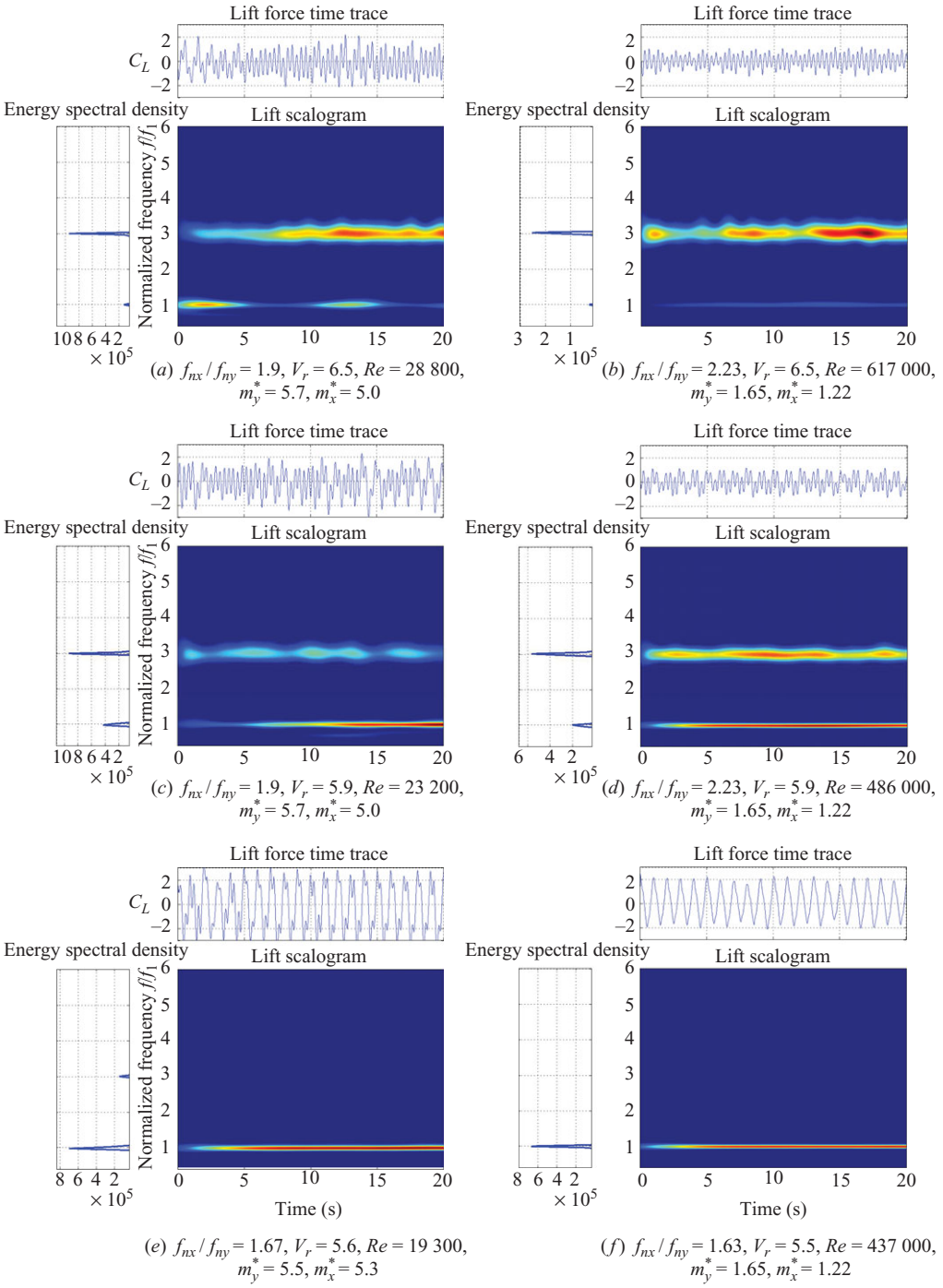

(*a*) $f_{nx}/f_{ny} = 1.9$, $V_r = 6.5$, $Re = 28\,800$, $m_y^* = 5.7$, $m_x^* = 5.0$

(*b*) $f_{nx}/f_{ny} = 2.23$, $V_r = 6.5$, $Re = 617\,000$, $m_y^* = 1.65$, $m_x^* = 1.22$

(*c*) $f_{nx}/f_{ny} = 1.9$, $V_r = 5.9$, $Re = 23\,200$, $m_y^* = 5.7$, $m_x^* = 5.0$

(*d*) $f_{nx}/f_{ny} = 2.23$, $V_r = 5.9$, $Re = 486\,000$, $m_y^* = 1.65$, $m_x^* = 1.22$

(*e*) $f_{nx}/f_{ny} = 1.67$, $V_r = 5.6$, $Re = 19\,300$, $m_y^* = 5.5$, $m_x^* = 5.3$

(*f*) $f_{nx}/f_{ny} = 1.63$, $V_r = 5.5$, $Re = 437\,000$, $m_y^* = 1.65$, $m_x^* = 1.22$

FIGURE 4. Scalogram showing the instantaneous frequency components of lift for sample low- and high-Reynolds-number cases. Frequency is normalized by the dominant motion frequency, f_1. The first- and third-harmonic components of lift are clearly visible in each scalogram.

instantaneous frequency information as a function of time in the form of a scalogram and (*b*) the power spectral density. A scalogram shows the squared magnitude of a continuous wavelet transform as a function of frequency and time (Boashash 2003). At a reduced velocity of 6.5, the power spectral density shows that lift is dominated by its third harmonic, with a small contribution from the first harmonic, for both low- and high-Reynolds-number cases. At high Reynolds number, however, the instantaneous frequency content shows relatively steady first- and third-harmonic components as a function of time, while at lower Reynolds number, the signal presents some fluctuations of the first and third harmonics, with the third harmonic primarily dominant.

In the low- and high-Reynolds-number pairs presented in figures 4(*a*) and 4(*b*), the third harmonic is the dominant component of lift, yet the relative strength of the lift harmonics is slightly different. This we attribute to the fact that lift forces are strongly dependent on the vortex formation near the cylinder and in the wake, which are influenced, in turn, by the features of the orbital motion of the cylinder (Dahl, Hover & Triantafyllou 2008). As a result, the small differences in magnitude and phase between the low- and high-Reynolds-number responses can lead to the differences noted in the lift harmonics.

The drag force signals shown in figure 3 are similar for reduced velocity of 5.9, with a dominant frequency at twice the crossflow oscillation frequency. For the cases with reduced velocity near 5.5, the drag signals are quite different because of difference in the magnitude of in-line and crossflow motions. Again, this motion difference plays a critical role in defining the forces exerted on the body. For reduced velocity of 6.5, the mean drag in the low-Reynolds-number case is slightly higher than for the high-Reynolds-number case. It must be noted that the Reynolds number of 617 000 is well above the boundary layer transition *Re* for a stationary cylinder; hence the wake is narrower than for the subcritical case at a Reynolds number of 28 800. We must also note that the high-*Re* case results are for a rough cylinder.

3.1. *Dual resonance and third-harmonic lift*

Previous studies have shown that a combined in-line and crossflow vibration of a cylinder can result in significant third-harmonic components of lift (Jauvtis & Williamson 2004; Dahl *et al.* 2007). For particular values of the ratio of in-line versus transverse natural frequencies, the third harmonic may even dominate over the first harmonic (Dahl *et al.* 2007). The orbital shape of the motion is critical in defining the amplitude and frequency content of these forces (Dahl *et al.* 2008). In the following figures the orbit of the cylinder is shown in a reference frame fixed with respect to the towing carriage. This plot is effective in illustrating the phase difference, θ, between the crossflow and the in-line response.

Figure 5 shows the orbits measured for the high-Reynolds-number experiments, plotted using first the nominal reduced velocity and then the true reduced velocity. The nominal reduced velocity is defined using the nominal natural frequency, while the true reduced velocity is defined on the basis of the effective natural frequency of the system. This effective natural frequency takes into account the fluid forces in phase with acceleration acting on the cylinder. The background contours depict the ratio of the third-harmonic lift coefficient over the total peak lift coefficient. In figure 5(*a*), the nominal reduced velocity spreads the data across the entire experimental range, since for each value of V_{rn} there is a corresponding unique run. There are cases of figure-eight motion when the cylinder moves upstream at the two extremes of the orbit (top and bottom); this orbital motion was termed a 'counterclockwise motion' in (Dahl *et al.* 2007), since the cylinder motion is counterclockwise at the top of the figure-eight

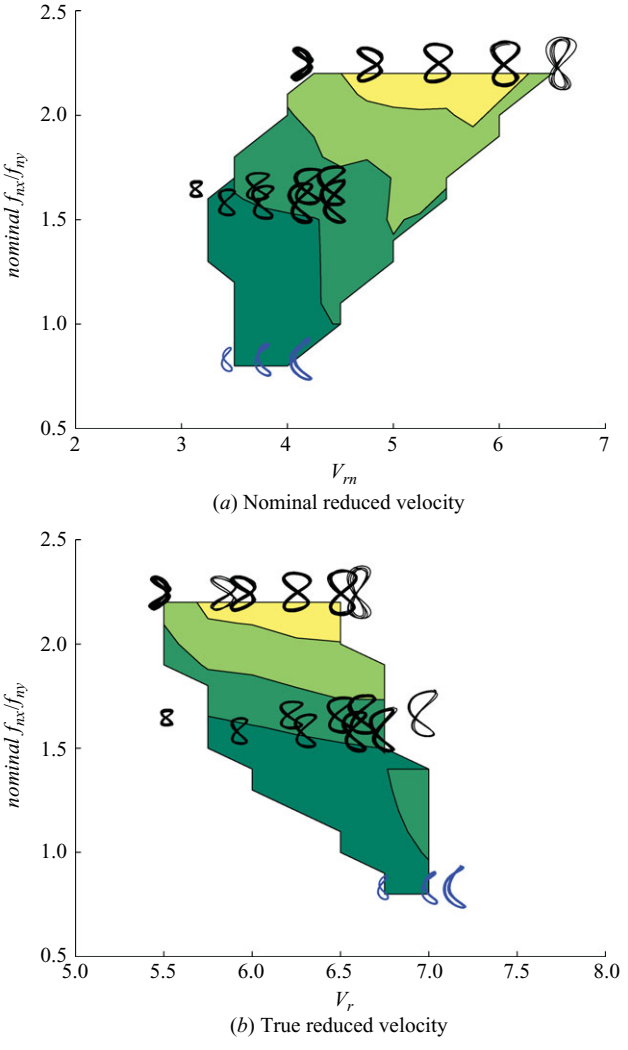

FIGURE 5. Cylinder orbital trajectories versus the nominal natural-frequency ratio and the (*a*) nominal reduced velocity and (*b*) the true reduced velocity. Blue: trajectory moves downstream at the top of the figure-eight (clockwise). Black: trajectory moves upstream at the top of figure-eight (counterclockwise). The flow is left to right. The contours provide the third-harmonic lift coefficient as fraction of the total lift coefficient for the high-Reynolds-number experiments. Darkest green denotes a lift third harmonic less than 25 % of total lift; yellow denotes a lift third harmonic greater than 75 % of total lift.

orbit. This type of motion is associated with large third-harmonic forces. In contrast, a downstream-facing crescent orbit, or a clockwise figure-eight motion, is indicative of stronger first-harmonic forces relative to the total lift magnitude. Although the nominal parameters are useful at uniquely representing the data, they provide neither insight on the resonance properties of the structure nor scalable non-dimensional frequencies to allow comparison between different-scale experiments. It is, therefore, important to also consider the motions and forces exerted on the cylinder in terms of the true reduced velocity.

Figure 5(*b*) shows two particular features of the response at high Reynolds number. First, the phase between in-line and crossflow motions varies with true reduced

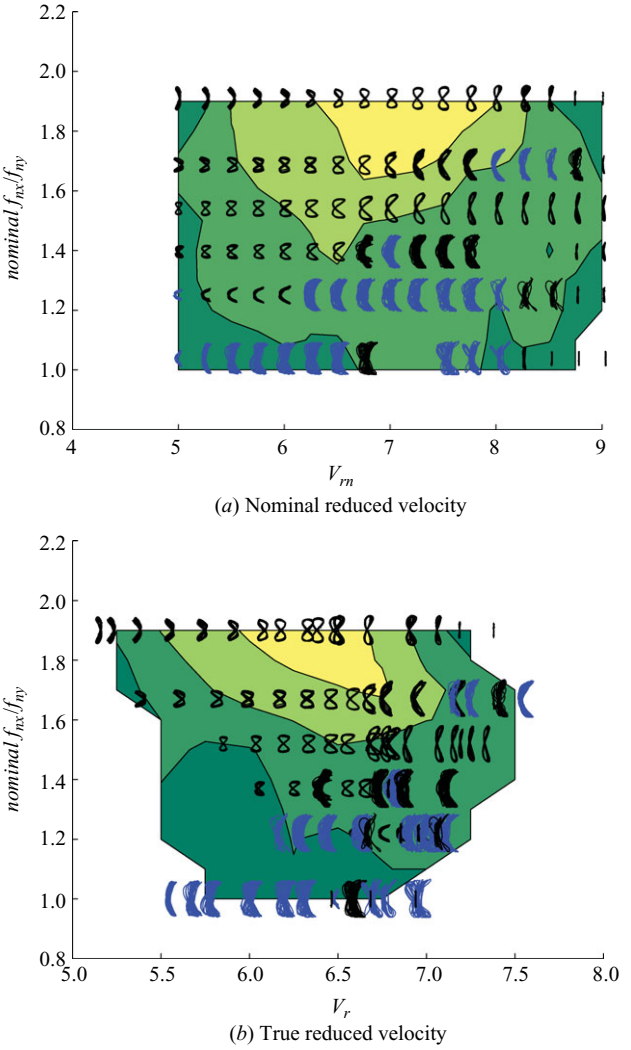

FIGURE 6. Cylinder orbital trajectories versus the nominal natural-frequency ratio and the (*a*) nominal reduced velocity and (*b*) the true reduced velocity. Blue: trajectory moves downstream at the top of the figure-eight (clockwise). Black: trajectory moves upstream at the top of figure-eight (counterclockwise). The flow is left to right. Orbits are overlaid on contours depicting the third lift harmonic as fraction of total lift force for the low-Reynolds-number experiments. Darkest green denotes a third-harmonic magnitude less than 25 % of the total lift; yellow denotes a third-harmonic magnitude greater than 75 % of the total lift.

velocity. At low reduced velocities, the shape of the orbit is curved upstream, while at high reduced velocity the shape is curved downstream. The second feature is that a local maximum of the third-harmonic forces occurs at reduced velocity of 6.4, when associated with a nominal natural-frequency ratio that is near 2. Within this region, the third-harmonic forces become the dominant component of lift, accompanied by purely figure-eight, counterclockwise orbital motions of the cylinder.

At low Reynolds numbers we can make nearly identical observations. Figure 6 shows the orbital shapes and third-harmonic contours for the nominal and effective reduced velocities in the low-Reynolds-number experiments. Again, the nominal

reduced velocity uniquely represents the low-Reynolds-number set, clearly showing the orbital motions and contours of the third-harmonic lift over the entire test matrix. A region of dominant third-harmonic lift occurs for a nominal natural-frequency ratio of 1.9. The data collapse into a smaller parametric range, again, when plotted as a function of the true reduced velocity. In the low-Reynolds-number set, many of the orbital shapes with nominal natural-frequency ratio near 1 appear fairly messy because the in-line motion did not settle into a regular, repeatable oscillation. The crossflow oscillation at these lower nominal frequency ratios did, however, show regular, repeatable response with a frequency close to the Strouhal value.

The contour plot of the lift third-harmonic component as a fraction of the total lift is similar to the corresponding plot for high Reynolds number. A local maximum of the percentage of third-harmonic lift occurs at the reduced velocity of 6.4, when the nominal natural-frequency ratio is near 2. The region of dominant third-harmonic lift forces is, again, associated with figure-eight counterclockwise orbits, implying that low- and high-Reynolds-number wake patterns must be similar as well.

3.1.1. *Effective natural frequency*

The effective natural frequencies are found using the effective rather than the nominal added mass coefficient, calculated from the fluid force in phase with acceleration. Since the crossflow cylinder motion is harmonic in these experiments, the force in phase with acceleration depends only on the first-harmonic component of the lift force. Similarly, the in-line motion of the cylinder occurs at twice the frequency of the crossflow motion, and hence the in-line force in phase with acceleration is only a function of the second-harmonic fluctuating drag force. The lift and drag forces can be decomposed into forces in phase with acceleration and velocity, as in Sarpkaya (1979) and Bearman (1984).

The effective added mass m_{ea} is added to the measured system mass to define the effective natural frequency for a given experimental run, as shown in (3.1). This equation can be derived directly from the linear equation of motion, assuming the forcing frequency is the same as that of the body motion. A different effective mass can be determined for in-line and crossflow motions; so the natural frequencies for in-line and crossflow motions are adjusted separately. The ratio of the in-line and crossflow effective natural frequencies is denoted in the figures as '*effective* f_{nx}/f_{ny}'. The effective natural frequency of the system is not a true natural frequency, as explained by Sarpkaya (2004), since the frequency is dependent on the dynamic forces exerted on the body; however, it is useful for characterizing the near-resonant response of the system. 'Dual resonance' can then be defined as a condition in which the system is resonant with both the effective in-line natural frequency and the effective crossflow natural frequency. These effective natural frequencies are equivalent to the observed oscillation frequency of the cylinder in the in-line and crossflow directions:

$$\textit{effective}\, f_n = \sqrt{\frac{k}{m + m_{ea}}}. \tag{3.1}$$

Figure 7(*a*) shows the orbit shapes for all experiments, plotted versus (*a*) the effective natural-frequency ratio and (*b*) the true reduced velocity. The direction of orbit (clockwise versus counterclockwise), and high-Reynolds-number cases versus low-Reynolds-number cases are distinguished by colour. For most experiments shown, regardless of the nominal natural-frequency ratio, the responses collapse to an effective natural-frequency ratio close to 2; previous experiments have observed the same phenomenon, even when the nominal natural-frequency ratio was far from

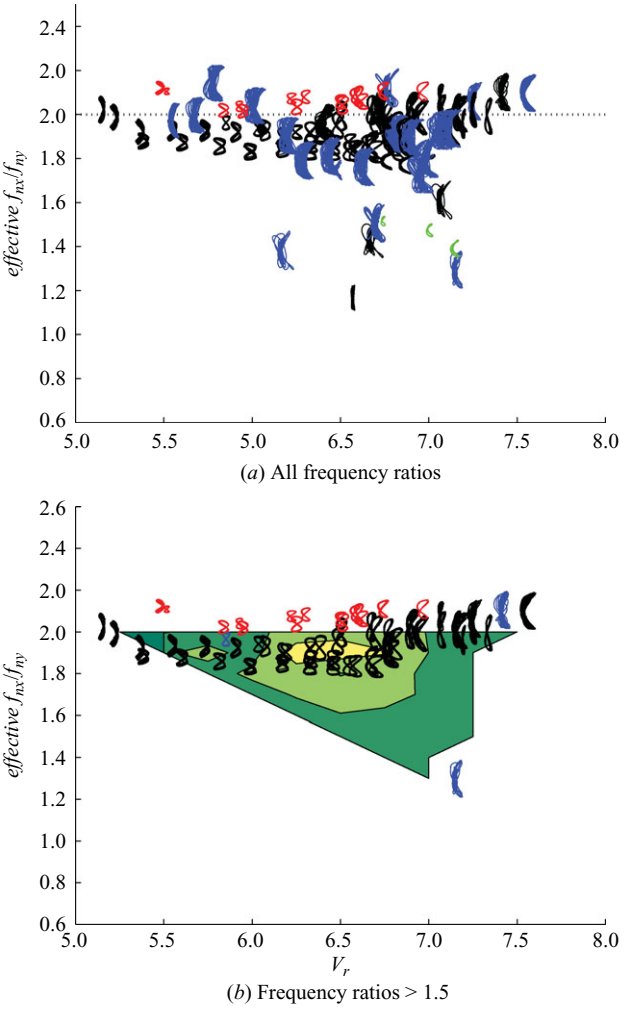

FIGURE 7. Combined high- and low-Reynolds-number orbital trajectories. (*a*) All orbits from high- and low-*Re* experiments against the effective natural-frequency ratio. Regardless of the nominal frequency ratio, the effective natural-frequency ratios tends to 2. (*b*) Only orbits with a nominal frequency ratio higher than 1.5, overlaid on contours depicting the third-harmonic lift as a fraction of the total lift for the low-Reynolds-number experiments. Blue (clockwise) and black (counterclockwise) trajectories are low-Reynolds-number cases, while green (clockwise) and red (counterclockwise) trajectories indicate high-Reynolds-number cases. The contours are equivalent to figures 5 and 6.

2 (Sarpkaya 1995; Jauvtis & Williamson 2004). It is interesting that in figure 7(*a*) some of the cases exhibiting irregular cylinder motions also reach an effective natural frequency near 2. In these cases, the effective added mass is calculated on a per-cycle basis, using the regular, crossflow motion to define each cycle. There are also some cases in which the effective natural frequency did not reach a value close to 2.

It is well known that the vortex formation process in the cylinder wake results in a forcing mechanism in which the in-line fluid force has half the period of the crossflow force. In addition, we find in the majority of the present experiments that as the body interacts dynamically with its wake, the system reaches a dynamic equilibrium, where the in-line and crossflow effective added masses are such that the effective

natural-frequency ratio is close to 2. This result has previously been noted (Sarpkaya 1995; Jauvtis & Williamson 2004) and is remarkable because it is so persistent, and yet it cannot be anticipated on the basis of any principle of mechanics. It must be clarified that a system with a nominal natural-frequency ratio sufficiently far from the value 2 may never get close to an effective natural-frequency ratio of 2 because the necessary combination of effective crossflow and in-line added masses is not possible to reach. In such cases, the orbit may be either oddly shaped or unstable and non-repeatable, as seen in some cases in figure 7(*a*). In contrast, repeatable motions of the cylinder typically indicate a resonant condition in which the effective natural-frequency ratio is near 2.

Figure 7(*b*) shows the orbital shapes from both experimental sets; cases with nominal frequency ratios near 1 were removed for clarity. If we consider only frequency ratios greater than 1.5, it is possible to obtain a unique parametric collapse to a region in which the third harmonic is dominant, and the true reduced velocity is in a narrow range around 6.4. We show only contours of the third lift harmonic to total lift ratio for the low-Reynolds-number experiments because the high-Reynolds-number contours are very similar.

Overall, the motions of the cylinder at high and low Reynolds numbers are similar, but the high-*Re* crossflow motions are smaller by about 20 %. The third lift harmonic as percentage of the total lift is the same between the subcritical and supercritical cases, despite the differences in motion and force amplitudes. The orbit shapes are similar as well, for the same values of the reduced velocity. As reduced velocity increases, the phase between in-line and crossflow motions changes such that the orbit goes from a C-shaped orbit with upstream-facing lobes to a C-shaped orbit with downstream-facing lobes. The orbit shapes are stable and highly repeatable in every case.

3.2. *Cylinder motions*

A direct comparison between the motions and forces observed for the high- and low-Reynolds-number experiments shows strong similarities between the two data sets. Despite differences in surface roughness, mass ratio and system damping, the two experiments exhibit similar trends in the fundamental response and forces observed at low and high Reynolds numbers. Although several nominal natural-frequency ratios were tested for low *Re*, we focus on the frequency ratios with nominal values closer to two, for which high-*Re* tests are also available. In the following cases, we compare the low-Reynolds-number cases with nominal $f_{nx}/f_{ny} = 1.9$ and high-*Re* cases with nominal $f_{nx}/f_{ny} = 2.2$. Similarly, a comparison is made between the low-*Re* experiments with nominal $f_{nx}/f_{ny} = 1.67$ and the high-*Re* experiments with nominal $f_{nx}/f_{ny} = 1.63$.

3.2.1. *Cylinder response amplitudes*

The amplitudes of motion of the cylinder in the in-line and crossflow directions are presented as the statistical average of the highest 10 % of response amplitudes, consistent with the practice of Hover, Techet & Triantafyllou (1998). Figure 8 shows the amplitude of response in the crossflow direction for selected nominal natural-frequency ratios. The in-line response for the same frequency ratios is shown in figure 9.

At low Reynolds numbers, Sarpkaya (1995) first observed that two distinct peaks in the response amplitude occur as a function of the reduced velocity, for frequency ratios close to 2. Similar twin peaks were observed by Dahl *et al.* (2006), and these response amplitudes are compared with the high-*Re* experiments of the present study in figure 8. Figure 8 shows the low-*Re* response over the same range of nominal

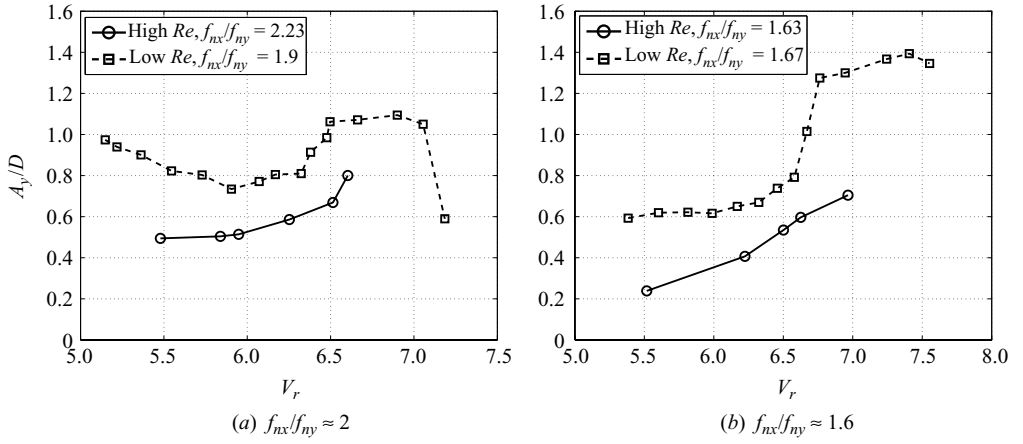

FIGURE 8. Comparison of crossflow amplitudes A_y/D for comparable nominal natural-frequency ratios: $m_y^* = 1.65$ ($f_{nx}/f_{ny} = 2.23$), 5.7 ($f_{nx}/f_{ny} = 1.9$), 1.65 ($f_{nx}/f_{ny} = 1.63$), 5.5 ($f_{nx}/f_{ny} = 1.67$).

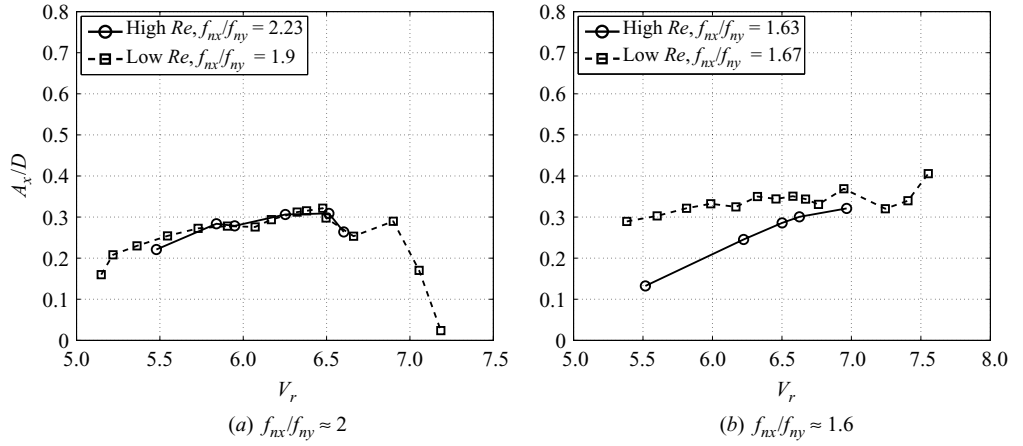

FIGURE 9. Comparison of in-line amplitudes A_x/D for comparable nominal natural-frequency ratios: $m_y^* = 1.65$ ($f_{nx}/f_{ny} = 2.23$), 5.7 ($f_{nx}/f_{ny} = 1.9$), 1.65 ($f_{nx}/f_{ny} = 1.63$), 5.5 ($f_{nx}/f_{ny} = 1.67$).

reduced velocities over which the high-*Re* experiments are available; hence only a portion of the first peak is shown near $V_r \approx 5.2$, with the second peak occurring near $V_r \approx 6.8$. In the high-Reynolds-number experiments, it is difficult to assess whether the two peaks occur at the same reduced velocity because of the relatively small number of data points; the data, however, show that the crossflow motion increases as the reduced velocity increases towards 7. As noted earlier, the crossflow amplitudes are smaller by about 20 % for the high-*Re* data; the same trend was found in the high-*Re* data of Ding *et al.* (2004), obtained for a cylinder allowed to oscillate only in the transverse direction. At the lower nominal natural-frequency ratio, the amplitudes of crossflow motion are also comparable between the low- and high-Reynolds-number cases, but the high-*Re* data are consistently smaller in magnitude.

The in-line motion of the cylinder is critically important when the system undergoes dual resonance, since it can significantly alter the vortex patterns and hence the measured forces on the cylinder. In the comparison shown in figure 9, the in-line

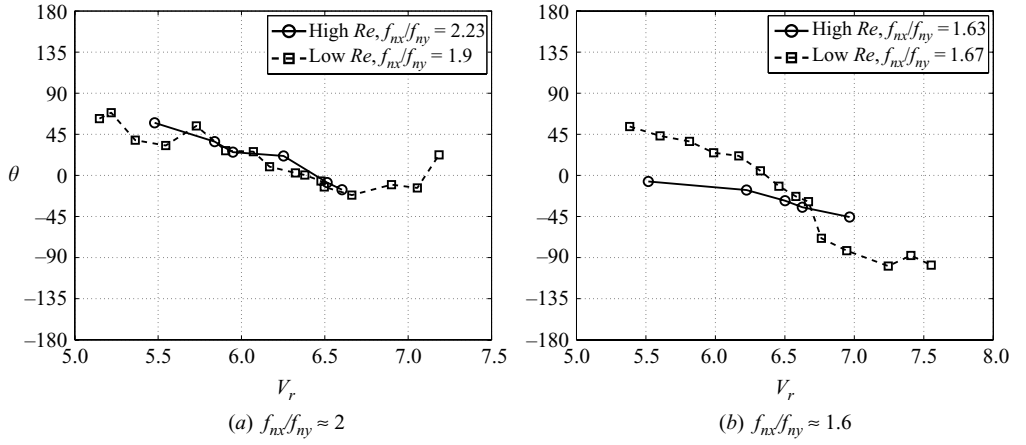

FIGURE 10. Comparison of phase between in-line and crossflow motions, θ, for comparable nominal natural-frequency ratios: $m_y^* = 1.65$ ($f_{nx}/f_{ny} = 2.23$), 5.7 ($f_{nx}/f_{ny} = 1.9$), 1.65 ($f_{nx}/f_{ny} = 1.63$), 5.5 ($f_{nx}/f_{ny} = 1.67$).

amplitude of motion is comparable for low and high Re, with maximum values near 0.3 cylinder diameters. The in-line motions are nearly identical for nominal natural-frequency ratios near 2.

3.2.2. *Phase between in-line and crossflow motions*

The phase between in-line and crossflow motions determines the orbital pattern (clockwise versus counterclockwise) and plays a significant role in the vortex formation process. As shown in figure 10, this phase is nearly the same for low- and high-Re data when the nominal frequency ratio is close to 2. For a nominal frequency of 1.6, the phases follow the same trend, but there are quantitative differences.

3.3. *Forces on the cylinder*

In one-degree-of-freedom VIV experiments, the dominant lift force occurs primarily at the fundamental frequency of cylinder motion; this is not true for two-degree-of-freedom experiments. Higher harmonic components of lift and drag must be accounted for, as these components of lift comprise a dominant portion of the lift coefficient at certain ranges of the reduced velocities. The lift forces acting on the body can be represented as a Fourier series consisting of odd harmonics; (3.2) provides a model for the hydrodynamic lift that includes a third-harmonic component. A fifth harmonic may also be present in the lift force, although in the present experiments the fifth-harmonic forces were found to be negligible. Equation (3.3) provides a similar representation of the drag force with a mean drag combined with fluctuating even harmonic components of drag:

$$C_L = C_{L1}\cos(\omega t + \phi_1) + C_{L3}\cos(3\omega t + \phi_3) + \ldots, \tag{3.2}$$

$$C_D = C_{Dmean} + C_{D2}\cos(2\omega t + \phi_2) + \ldots. \tag{3.3}$$

The phases shown in (3.2) are referenced to the cylinder motion. In particular, ϕ_1 is the phase between the first-harmonic force and the transverse harmonic motion; ϕ_3 refers to the phase between third-harmonic force and first-harmonic transverse motion. It should be mentioned that the crossflow motion has negligible third-harmonic component. In this paper, we focus primarily on the magnitudes C_{L1} and

C_{L3}, although the phasing between these components can significantly alter the peak magnitude of the total lift force.

The crossflow added mass coefficient is determined on the basis of the first-harmonic component of lift. The third-harmonic lift force is orthogonal to the first-harmonic motion; hence the effective added mass in the crossflow direction is defined exactly as for a cylinder oscillating in the crossflow direction only (as in Sarpkaya 1979 and Bearman 1984). Equation (3.4) provides the equation for the crossflow added mass:

$$C_{my} = \frac{-2U^2 C_{L1}\cos(\phi_1)}{\pi(A_y/D)D^2(2\pi f_y)^2}. \tag{3.4}$$

The added mass in the in-line direction can be calculated on the basis of the second harmonic of the fluctuating drag force in analogy with C_{my}:

$$C_{mx} = \frac{-2U^2 C_{D2}\cos(\phi_2)}{\pi(A_x/D)D^2(2\pi f_x)^2}. \tag{3.5}$$

Since the effective added mass depends on the amplitude and frequency of response, it can vary with time if these response features are not constant; hence, in a non-stationary response, the added mass may vary from cycle to cycle. Herein, in order to determine a single added mass that is representative of a given experimental run, the added mass is first calculated on a per-cycle basis, and then it is averaged over all cycles.

3.3.1. *Effective added mass coefficients*

The effective fluid added mass force changes the effective mass of the system, resulting in an effective natural frequency. The body motion becomes resonant, and the system oscillates at its effective natural frequency, although the nominal natural frequency may be distant from the frequency of vortex shedding. This is well known to occur for a cylinder constrained to crossflow motion (Sarpkaya 2004; Williamson & Govardhan 2004). In the case of two-degree-of-freedom response, such resonance caused by changes in the effective added mass can occur in both the in-line and the crossflow direction (dual resonance). The only constraint is that the frequency of excitation in the in-line direction is twice the frequency of the crossflow excitation.

In figure 11, the crossflow added mass of the high- and low-Reynolds-number tests are shown to be very similar for nominal natural-frequency ratios near 2. For frequency ratios near 1.67, there are larger deviations, although the trends are similar. It should be noted that a difference in the mass ratio plays a larger role for a frequency ratio of 1.67, because a larger variation in added mass is needed in order to drive the effective natural-frequency ratio to a value of 2. Indeed, in two different systems undergoing VIV and having the same initial frequency ratio (far from a value of 2) but different mass ratio, the respective added mass values required to drive the effective natural-frequency ratio to 2 will be necessarily different. In the low-Reynolds-number tests, the crossflow mass ratio was near a value of 5.7 and slightly smaller in the in-line direction, while for the high-Reynolds-number tests, mass ratios were significantly lower, less than 2.

In figure 12, the in-line added mass coefficients show also strong similarities between the low- and high-Reynolds-number tests. We conclude that in addition to significant variation of the crossflow effective added mass coefficients, there is also significant variation of the in-line added mass.

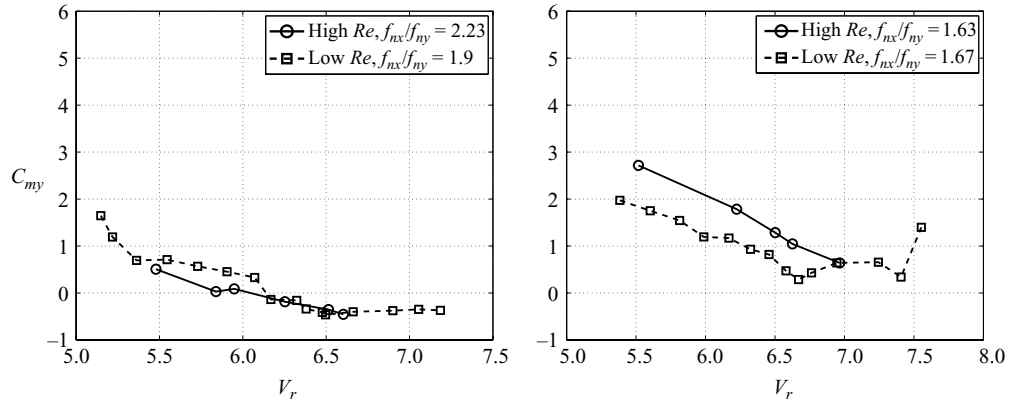

(*a*) $f_{nx}/f_{ny} \approx 2$ (*b*) $f_{nx}/f_{ny} \approx 1.6$

FIGURE 11. Comparison of crossflow effective added mass coefficients, C_{my}, for comparable nominal natural-frequency ratios: $m_y^* = 1.65$ ($f_{nx}/f_{ny} = 2.23$), 5.7 ($f_{nx}/f_{ny} = 1.9$), 1.65 ($f_{nx}/f_{ny} = 1.63$), 5.5 ($f_{nx}/f_{ny} = 1.67$).

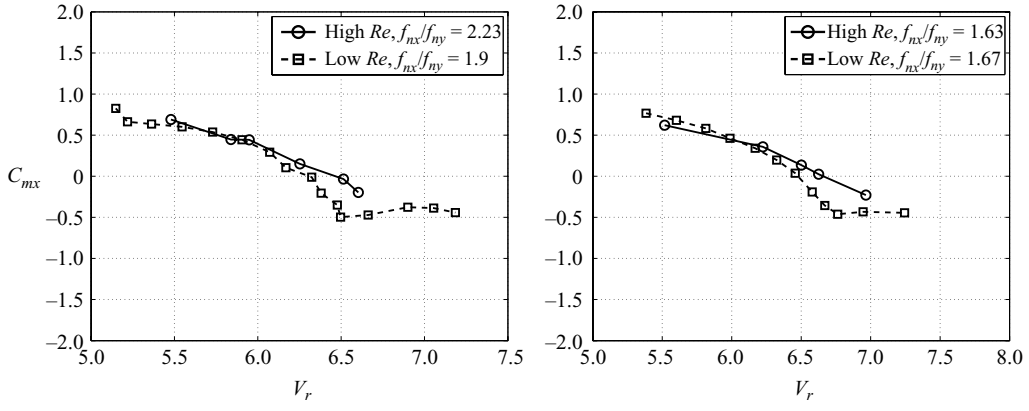

(*a*) $f_{nx}/f_{ny} \approx 2$ (*b*) $f_{nx}/f_{ny} \approx 1.6$

FIGURE 12. Comparison of in-line effective added mass coefficients, C_{mx}, for comparable nominal natural-frequency ratios: $m_y^* = 1.65$ ($f_{nx}/f_{ny} = 2.23$), 5.7 ($f_{nx}/f_{ny} = 1.9$), 1.65 ($f_{nx}/f_{ny} = 1.63$), 5.5 ($f_{nx}/f_{ny} = 1.67$).

3.3.2. *Lift coefficient*

The magnitude of the lift coefficient is a function of the in-line and crossflow responses, because both affect the vortex patterns in the wake. Figure 13 shows the magnitude of the first harmonic component of the lift force for the low- and high-Reynolds-number tests. A comparison between the exact values of the lift magnitude is not relevant, since the crossflow responses are not equal; however it is important to note that in both cases, the lift coefficient magnitudes are fairly large, indicating significant excitation of the cylinder in crossflow. The magnitude of the high-Reynolds-number forces are slightly smaller than the low-Reynolds-number forces because of smaller crossflow motions of the test cylinder and a narrower wake. In both cases with nominal natural-frequency ratios near 2, the first-harmonic magnitude is larger at low reduced velocities and decreases as reduced velocity increases. A minimum in the

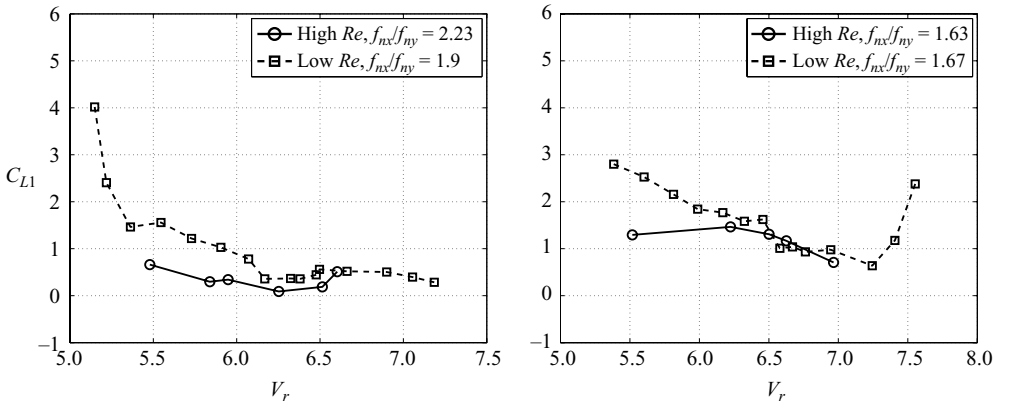

FIGURE 13. Comparison of first harmonic lift coefficient magnitude, C_{L1}, for comparable nominal natural-frequency ratios: $m_y^* = 1.65$ ($f_{nx}/f_{ny} = 2.23$), 5.7 ($f_{nx}/f_{ny} = 1.9$), 1.65 ($f_{nx}/f_{ny} = 1.63$), 5.5 ($f_{nx}/f_{ny} = 1.67$).

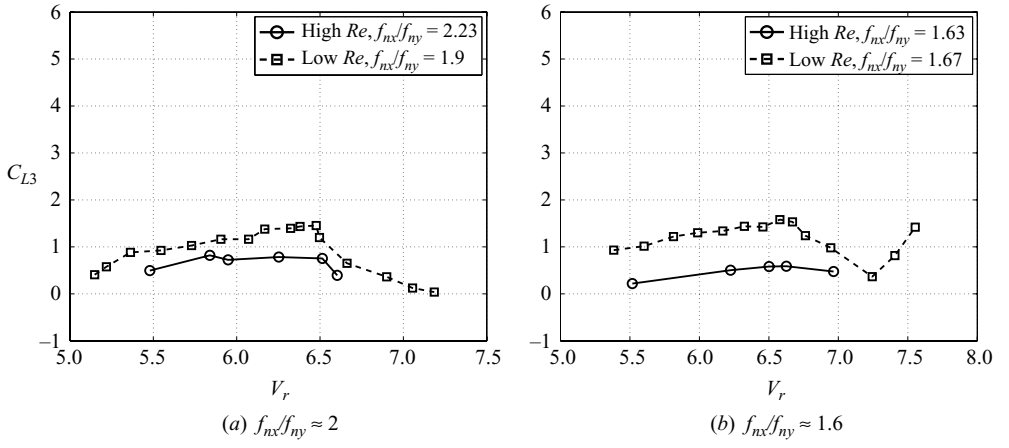

FIGURE 14. Comparison of third-harmonic lift coefficient magnitude, C_{L3}, for comparable nominal natural-frequency ratios: $m_y^* = 1.65$ ($f_{nx}/f_{ny} = 2.23$), 5.7 ($f_{nx}/f_{ny} = 1.9$), 1.65 ($f_{nx}/f_{ny} = 1.63$), 5.5 ($f_{nx}/f_{ny} = 1.67$).

first-harmonic component of force is reached near $V_r = 6.4$, where the third-harmonic component is at a maximum.

Figure 14 shows a comparison of the magnitudes of the third-harmonic components of lift. Again, the high-Reynolds-number magnitudes are slightly smaller than the low-Reynolds-number magnitudes; however, the same trends are observed for both data sets. It is interesting to note that although the magnitudes are different, figure 7 shows that the percentage of the third-harmonic lift coefficient over the total lift is roughly the same for both data sets.

The third-harmonic force does not contribute to significant excitation of the cylinder motion, since the frequency of the third-harmonic force is not close to a natural frequency of the structure. Third-harmonic motion response was observed to be negligible.

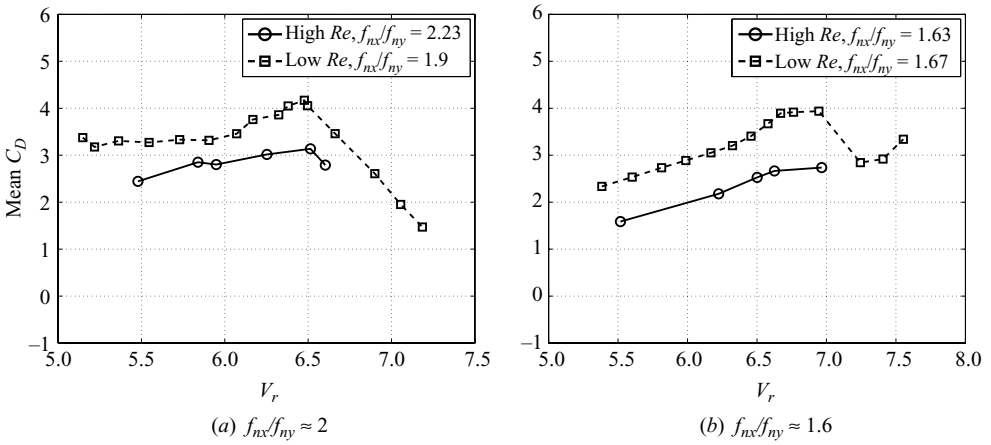

FIGURE 15. Comparison of mean drag coefficient for comparable nominal natural-frequency ratios: $m_y^* = 1.65$ ($f_{nx}/f_{ny} = 2.23$), 5.7 ($f_{nx}/f_{ny} = 1.9$), 1.65 ($f_{nx}/f_{ny} = 1.63$), 5.5 ($f_{nx}/f_{ny} = 1.67$).

3.3.3. *Drag coefficient*

For a rigid, smooth cylinder at supercritical Reynolds numbers, the mean drag coefficient is lower, around a value of 0.7, than for subcritical tests where the drag coefficient is closer to 1.2. The use of a roughened cylinder makes the difference in drag coefficient smaller. The mean drag coefficient for the supercritical experiments, when the cylinder was not allowed to oscillate, was measured to be near $C_D = 1.0$. When the cylinder is allowed to oscillate, in-line and crossflow motions cause the steady and unsteady drag coefficients to increase, with roughness affecting this amplification as well.

Figure 15 provides a comparison of the mean drag coefficients between the subcritical and the supercritical experiment. In general, the mean drag coefficient at higher Reynolds numbers is slightly smaller than for lower Reynolds numbers. At high Reynolds numbers, a smaller drag coefficient is also caused by the fact that the peak crossflow motion is found to be smaller by roughly 20–30 % than for subcritical tests.

Figure 16 shows the fluctuating drag component, which can often be quite large, as seen in both the low- and high-Reynolds-number cases. The fluctuating drag is defined as the total drag force minus the mean drag. The magnitude of the fluctuating drag is reported as the average of the top 10 % peak values. Similar overall trends are observed for both sets of experiments. The oscillatory drag coefficient is known to depend strongly on the amplitude of response; hence differences between high and low Re can be attributed to differences in amplitude of response.

3.3.4. *Phase between force and cylinder motion*

Figures 17 and 18 provide the phase angle between the lift force and the cross-flow motion and between the fluctuating drag force and the in-line motion, respectively. For both nominal frequency ratios of 2 and 1.6, the phases exhibit similar trends. It should be noted that the phase between the first-harmonic force and the crossflow motion is difficult to define when the third harmonic becomes dominant.

3.3.5. *Cross-correlation of spanwise lift*

The degree of correlated vortex formation along the span of the cylinder is an important factor in determining the magnitude of the cylinder response. A simple

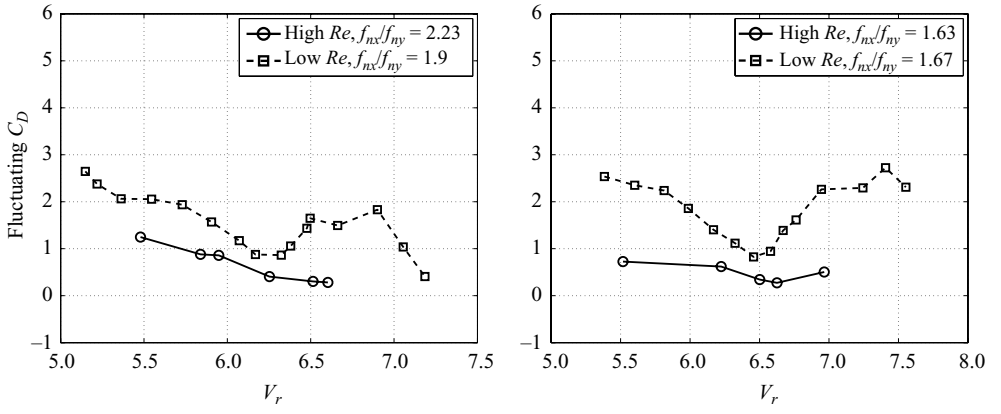

FIGURE 16. Comparison of fluctuating drag coefficient for comparable nominal natural-frequency ratios: $m_y^* = 1.65$ ($f_{nx}/f_{ny} = 2.23$), 5.7 ($f_{nx}/f_{ny} = 1.9$), 1.65 ($f_{nx}/f_{ny} = 1.63$), 5.5 ($f_{nx}/f_{ny} = 1.67$).

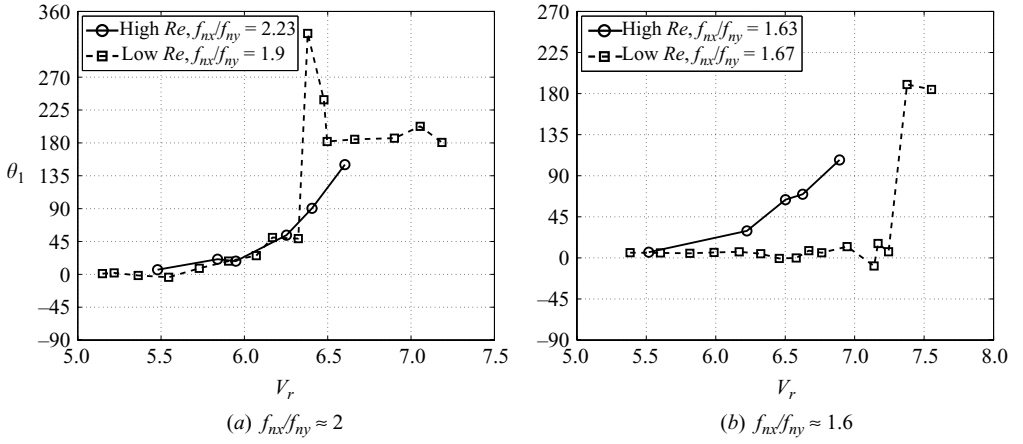

FIGURE 17. Comparison of phase between lift and crossflow motion, ϕ_1, for comparable nominal natural-frequency ratios: $m_y^* = 1.65$ ($f_{nx}/f_{ny} = 2.23$), 5.7 ($f_{nx}/f_{ny} = 1.9$), 1.65 ($f_{nx}/f_{ny} = 1.63$), 5.5 ($f_{nx}/f_{ny} = 1.67$).

measure of the spanwise correlation is the cross-correlation coefficient of the forces measured at the two ends of the cylinder. The study of Hover *et al.* (1998) showed that for a cylinder undergoing VIV in crossflow motion only, this cross-correlation coefficient maintains values near 1 (perfect correlation) over a relatively wide range of reduced velocity. The correlation dips to lower values in the reduced velocity region in which a wake transition is known to occur between '2S' and '2P' vortex patterns, as defined by Williamson & Roshko (1988). This transition region in the vortex patterns coincides with the peak VIV response of the cylinder; hence we find the paradoxical result that in the region of peak response the end forces have low correlation.

It is interesting, then, to investigate if a similar correlation dip exists for two-degree-of-freedom response. In our low-Reynolds-number experiments only one force sensor was used; hence it is not possible to estimate the cross-correlation, but for

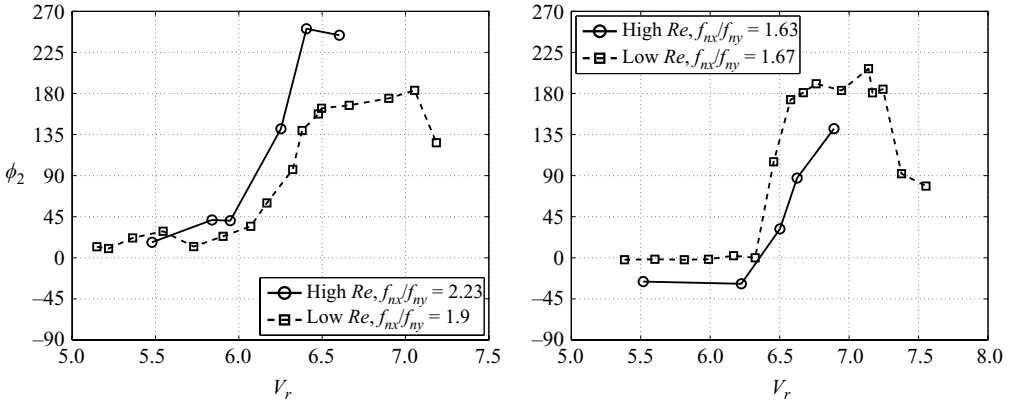

(*a*) $f_{nx}/f_{ny} \approx 2$ (*b*) $f_{nx}/f_{ny} \approx 1.6$

FIGURE 18. Comparison of phase between fluctuating drag and in-line motion, ϕ_2, for comparable nominal natural-frequency ratios: $m_y^* = 1.65$ ($f_{nx}/f_{ny} = 2.23$), 5.7 ($f_{nx}/f_{ny} = 1.9$), 1.65 ($f_{nx}/f_{ny} = 1.63$), 5.5 ($f_{nx}/f_{ny} = 1.67$).

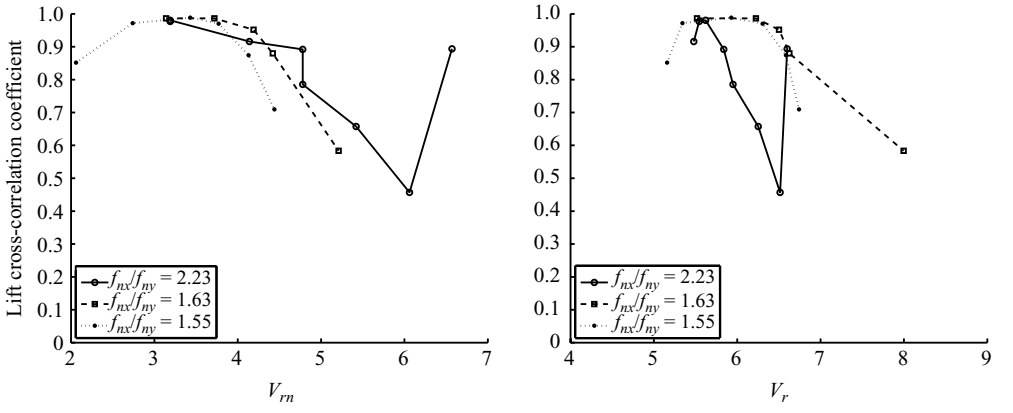

(*a*) Nominal reduced velocity (*b*) True reduced velocity

FIGURE 19. Cross-correlation coefficient for measured lift forces in the high-Reynolds-number apparatus.

the high-*Re* data this calculation is possible. Figure 19 shows the cross-correlation coefficient based on lift measurements from two force sensors located at the ends of the cylinder for the high-Reynolds-number experiments, first shown as a function of the nominal reduced velocity and then versus the true reduced velocity.

For each nominal natural-frequency ratio, there is a slightly different trend of the cross-correlation coefficient, and this difference is attributable to the effect of natural-frequency ratio on the motion responses. Jeon & Gharib (2001) showed that the phase between the in-line and crossflow motions of the cylinder can alter the reduced velocity for which a transition between 2S and 2P shedding occurs; this explains the effect of the natural-frequency ratio on the onset of the correlation dip. Although there are few points in describing each curve from the high-Reynolds-number experiments, a clear drop in the correlation coefficient can be seen. For the particular case of $f_{nx}/f_{ny} = 2.23$, there are enough data to show the eventual recovery of the correlation coefficient for higher reduced velocities, in accord with the results of Hover *et al.*

(1998). There is a shift in the value of the reduced velocity where a drop-off of the correlation coefficient occurs as a function of the natural-frequency ratio. It should be mentioned that in two-degree-of-freedom tests, additional vortex formation patterns may appear, dependent on the particular cylinder motion (Jauvtis & Williamson 2004; Dahl *et al.* 2007), in the form of multiple vortex clusters (triplets, quadruplets and higher-order clusters); hence this loss of correlation cannot be directly attributable to 2S-to-2P transition and needs further study.

4. Discussion

The transition of a cylinder's boundary layer from laminar to turbulent flow, and the resulting changes to the wake, do not allow, in principle, the extrapolation of properties from subcritical to supercritical Reynolds numbers. Hence, experimental studies of supercritical-Reynolds-number VIV are important, despite their substantial cost owing to the use of large-scale apparatus. Recent findings of the importance of in-line motion on the overall VIV response at subcritical *Re* require that high-*Re* investigations be conducted as two-degree-of-freedom tests, further increasing the complexity of the experimental apparatus.

It is fortuitous that the basic features of the VIV response at low and high Reynolds number are similar, as shown in figure 7. Of particular significance is the similarity in the regular orbital shapes observed at both high and low Reynolds numbers, associated with a dual-resonance response of the structure. The collapse of a significant part of the two-degree-of-freedom high-*Re* data to a ratio of effective in-line and transverse natural frequencies close to 2 is important, as it shows that dual resonance continues beyond the boundary-layer transition region. This ratio of frequencies is achieved, as in the low-*Re* case because of the substantial variability in the effective in-line and transverse added mass coefficients as a function of the reduced velocity.

There is no principle of mechanics that can be used to explain why the flow–structure interaction process leads, in the majority of cases studied herein, to parametric combinations that provide an effective natural-frequency ratio $f_{nx}/f_{ny} \approx 2$. We note that when the nominal frequency ratio is sufficiently close to 2, then a dual resonance is guaranteed to occur. An interesting question is what are the upper and lower threshold values of the initial natural-frequency ratio that make this dual resonance still possible? The effective mass ratio in both directions, in-line and crossflow, is an important factor, since for mass ratios close to 1, changes in the effective added mass affect the total mass significantly. For example, Jauvtis & Williamson (2004) observed regular, repeatable orbit shapes with low mass ratios even for a nominal natural-frequency ratio of 1. In the present study, where the mass ratio is higher, when the nominal frequency ratio is sufficiently far from a value of 2, irregular orbit shapes are noted, and in some cases, dual resonance is not achieved.

The orbit shape is of particular importance because the motion of the cylinder through the fluid affects the resulting vortex patterns in the wake. When the cylinder performs a figure-eight motion and moves upstream at the two extreme ends of the orbit (counterclockwise motion), additional vorticity is generated, resulting in multiple vortex formation and high force harmonics (Dahl *et al.* 2007). This motion is also associated with stable orbits and dual resonance. We may conclude that the similarity in the orbits at subcritical and supercritical Reynolds numbers and in the fluid forces, established in this paper, imply similar vortex formation patterns.

We focus, in particular, on the region around the reduced velocity value of 6.4, when the nominal natural-frequency ratio is close to 2, resulting in dual resonance.

The third-harmonic component of the lift force dominates the first-harmonic force for both high and low Reynolds numbers. For subcritical tests, Dahl *et al.* (2008) used a simple potential flow construction to explain how the vortex formation pattern, observed for the associated counterclockwise orbital motion at $V_r = 6.4$, provides vortex forces which cancel both the lift and drag forces in phase with acceleration, resulting in an effective added mass close to zero in both the in-line and crossflow directions. When the structural damping is very low, the crossflow fluid force in phase with velocity must also be close to zero for free, steady-state oscillations to occur; hence, the entire first harmonic of the crossflow force must be near zero. This explains why in this particular regime, the third-harmonic lift force is the dominant component of the total lift force. This holds true at both the low and high Reynolds numbers and is further evidence that the vortex patterns at high Reynolds numbers are similar to those observed at low Reynolds numbers.

Although a large third lift harmonic force exists, no appreciable third-harmonic crossflow motion is observed at low or high *Re*. In the present experimental studies, this is attributed to the fact that the third-harmonic frequency is far from the natural frequency of the system, and hence excited motion at that frequency is very small. In a tension-dominated flexible cylinder undergoing VIV, there is a countable infinity of natural frequencies, at integer multiples of a fundamental one; hence, the third force harmonic may be close to a natural frequency. Even then, however, motions are found to be small. As explained in Mukundan (2008), for a flexible structure to be excited, it is not sufficient to simply excite a natural frequency; the force must have a spatial distribution in sympathy with the associated mode. Otherwise, if the force has the spatial distribution of a different mode, mode orthogonality results in a small response. Indeed, the third force harmonic was found to have similar spatial distribution as the first force harmonic along a flexible cylinder, resulting in small motion response (Mukundan 2008). Field experiments by Vandiver *et al.* (2009) along with lab experiments by Trim *et al.* (2005) have shown that flexible cylinders exhibit very small third-harmonic motions, despite the presence of large third-harmonic forces.

A systematic high-Reynolds-number investigation, especially involving flow visualization, is prohibitively expensive, as large facilities must be employed over long periods of time. As a result, the qualitative and quantitative agreement between the limited high-Reynolds-number tests and the more extensive lower-Reynolds-number tests, as found in this paper, is helpful in extrapolating known properties from a low-*Re* to a high-*Re* regime. We must note, again, that at smaller Reynolds number we used a smooth cylinder, while at supercritical Reynolds number we used a 0.23 % rough cylinder. As explained, this was done because a smooth cylinder in the critical-*Re* regime can be classified as 'pathological' in the sense that small variations in roughness cause large changes in response. The chosen roughness makes the responses stable but also affects the boundary layer and the separation points, making the lower-*Re* and higher-*Re* average wake width and mean drag coefficients rather similar.

5. Conclusions

The two-degree-of-freedom vortex-induced responses of an elastically mounted rigid cylinder within a crossflow are studied at subcritical Reynolds numbers between 15 000 to 60 000 on a smooth cylinder and at Reynolds numbers from 320 000 to 710 000 on a 0.23 % roughened cylinder. Responses are found to be similar despite differences in scale, experimental apparatus, mass ratio and system damping.

In most experimental cases considered, at both high and low Reynolds numbers, the cylinder response is characterized by 'dual resonance', a condition in which the lift force is resonant with the effective crossflow natural frequency, and the unsteady drag force is resonant with the effective in-line natural frequency. Dual resonance is possible over a wide parametric range because the effective crossflow and in-line added masses can vary significantly. Under dual-resonance conditions, large third-harmonic lift components were measured at high Reynolds number. Such third harmonics were first discovered in the subcritical regime.

The shape of the cylinder orbital motion affects the fluid force amplitude and frequency content and is determined by the phase between in-line and crossflow motion. The phase for high Re is shown to be strongly related to the true reduced velocity and to be nearly the same as for low Reynolds numbers. As in subcritical tests, supercritical responses exhibit figure-eight orbits with significant transverse and in-line response. Orbits are typically stable, persisting for the entire duration of the test, as shown in figure 7. Some moderate quantitative differences are noted between low- and high-Reynolds-number cases, particularly in the crossflow motion amplitude and force magnitude.

The authors acknowledge with gratitude the permission by Deepstar to publish the high-Reynolds-number tests. Special thanks are due to Dr Don Spencer of Oceanic Consulting and the staff at Memorial University, St. John's, Canada, for expertly conducting the high-Reynolds-number experiments.

REFERENCES

Achenback, E. 1968 Distribution of local pressure and skin friction around a circular cylinder in crossflow up to $Re = 5 \times 10^6$. *J. Fluid Mech.* **34**, 525–539.

Allen, D. W. & Henning, D. L. 1997 Vortex-induced vibration tow tests of smooth cylinders at supercritical Reynolds numbers. In *Proceedings of the 7th International Offshore and Polar Engineering Conference*, pp. 680–685. ISOPE.

Bearman, P. W. 1969 On vortex shedding from a circular cylinder in the critical Reynolds number regime. *J. Fluid Mech.* **37** (3), 577–585.

Bearman, P. W. 1984 Vortex shedding from oscillating bluff bodies. *Annu. Rev. Fluid Mech.* **16**, 195–222.

Blevins, R. D. 1990 *Flow Induced Vibration*. Van Nostrand Reinhold.

Boashash, B. (Ed.) 2003 *Time Frequency Signal Analysis and Processing: A Comprehensive Reference*, 1st edn. Elsevier.

Carberry, J., Sheridan, J. & Rockwell, D. 2005 Controlled oscillations of a cylinder: forces and wake modes. *J. Fluid Mech.* **538**, 31–69.

Dahl, J. M., Hover, F. S. & Triantafyllou, M. S. 2006 Two-degree-of-freedom vortex-induced vibrations using a force assisted apparatus. *J. Fluids Struct.* **22**, 807–818.

Dahl, J. M., Hover, F. S. & Triantafyllou, M. S. 2008 Third harmonic lift forces from phase variation in forced crossflow and in-line cylinder motions. In *Ninth International Conference on Flow-Induced Vibrations*, Prague, Czech Republic.

Dahl, J. M., Hover, F. S., Triantafyllou, M. S., Dong, S. & Karniadakis, G. E. 2007 Resonant vibrations of bluff bodies cause multi-vortex shedding. *Phys. Rev. Lett.* **99** (144503).

Ding, Z. J., Balasubramanian, S., Lokken, R. T. & Yung, T.-W. 2004 Lift and damping characteristics of bare and straked cylinders at riser scale Reynolds numbers. In *Offshore Technology Conference*, OTC-16341, Houston, TX.

Govardhan, R. N. & Williamson, C. H. K. 2006 Defining the 'modified Griffin plot' in vortex-induced vibration: revealing the effect of Reynolds number using controlled damping. *J. Fluid Mech.* **561**, 147–180.

Hover, F. S., Techet, A. H. & Triantafyllou, M. S. 1998 Forces on oscillating uniform and tapered cylinders in crossflow. *J. Fluid Mech.* **363**, 97–114.

James, W. D., Paris, S. W. & Malcolm, G. N. 1980 Study of viscous crossflow effects on circular cylinders at high Reynolds numbers. *AIAA J.* **18** (9), 1066–1072.

Jauvtis, N. & Williamson, C. H. K. 2004 The effect of two degrees of freedom on vortex-induced vibration at low mass and damping. *J. Fluid Mech.* **509**, 23–62.

Jeon, D. & Gharib, M. 2001 On circular cylinders undergoing two-degree-of-freedom forced motions. *J. Fluids Struct.* **15**, 533–541.

Klamo, J. T., Leonard, A. & Roshko, A. 2005 On the maximum amplitude for a freely vibrating cylinder in crossflow. *J. Fluids Struct.* **21** (4), 429–434.

Lucor, D., Mukundan, H. & Triantafyllou, M. S. 2006 Riser modal identification in CFD and full-scale experiments. *J. Fluids Struct.* **22**, 905–917.

Mukundan, H. 2008 Vortex-induced vibration of marine risers: motion and force reconstruction from field and experimental data. PhD thesis, Massachusetts Institute of Technology, Cambridge, MA.

Mukundan, H., Hover, F. S. & Triantafyllou, M. S. 2009 Applications of accurate viv response reconstruction schemes. In *International Conference on Ocean, Offshore and Arctic Engineering, OMAE'09*. Honolulu, HI, paper no. 79948.

Raghavan, K. & Bernitsas, M. M. 2007 Enhancement of high damping VIV through roughness distribution for energy harnessing at $8 \times 10^3 < Re < 1.5 \times 10^5$. In *Fifth Conference on Bluff Body Wakes and Vortex-Induced Vibrations*, Costa do Saupe, Bahia, Brazil.

Roshko, A. 1961 Experiments on the flow past a circular cylinder at very high Reynolds number. *J. Fluid Mech.* **10**, 345–356.

Sarpkaya, T. 1979 Vortex induced oscillations. *J. Appl. Mech.* **46**, 241–258.

Sarpkaya, T. 1995 Hydrodynamic damping, flow-induced oscillations, and biharmonic response. *J. Offshore Mech. Arct. Engng* **117**, 232–238.

Sarpkaya, T. 2004 A critical review of the intrinsic nature of vortex-induced vibrations. *J. Fluids Struct.* **19**, 389–447.

Schewe, G. 1983 On the force fluctuations acting on a circular cylinder in crossflow from subcritical up to transcritical Reynolds numbers. *J. Fluid Mech.* **133**, 265–285.

Shih, W. C. L., Wang, C., Coles, D. & Roshko, A. 1993 Experiments on flow past rough circular cylinders at large Reynolds numbers. *J. Wind Engng Indus. Aerodyn.* **49**, 351–368.

Szechenyi, E. 1975 Supercritical Reynolds number simulation for two-dimensional flow over circular cylinders. *J. Fluid Mech.* **70** (3), 529–542.

Triantafyllou, M. S., Dahl, J., Mukundan, H. & Hover, F. 2007 Recent conceptual developments in vortex-induced vibrations. In *International Conference on Ocean, Offshore and Arctic Engineering, OMAE'07*, San Diego, CA.

Trim, A. D., Braaten, H., Lie, H. & Tognarelli, M. A. 2005 Experimental investigation of vortex-induced vibration of long marine risers. *J. Fluids Struct.* **21**, 335–361.

Vandiver, J. K., Jaiswal, V. & Jhingran, V. 2009 Insights on vortex-induced travelling waves on long risers. *J. Fluids Struct.* **25**, 641–653.

Vandiver, J. K., Swithenbank, S., Jaiswal, V. & Jhingran, V. 2006 Fatigue damage from high mode number vortex-induced vibration. In *25th International Conferenece on Offshore Mechanical and Arctic Engineering*, Hamburg, Germany.

Williamson, C. H. K. & Roshko, A. 1988 Vortex formation in the wake of an oscillating cylinder. *J. Fluids Struct.* **2**, 355–381.

Williamson, C. H. K. & Govardhan, R. 2004 Vortex-induced vibrations. *Annu. Rev. Fluid Mech.* **36**, 413–455.

Zan, S. J. 2008 Experiments on circular cylinders in crossflow at Reynolds numbers up to 7 million. *J. Wind Engng Indus. Aerodyn.* **96**, 880–886.

Zan, S. J. & Matsuda, K. 2002 Steady and unsteady loading on a roughened circular cylinder at Reynolds numbers up to 900,000. *J. Wind Engng Indus. Aerodyn.* **90**, 567–581.

Zdravkovich, M. M. 1997 *Flow around Circular Cylinders, Volume1: Fundamentals*. Oxford University Press.